Air Force Institute of Technology
AFIT Scholar

Theses and Dissertations | Student Graduate Works

6-2007

# A Comparison of Film Cooling Techniques in a High Speed, True Scale, Fully Cooled Turbine Vane Ring

Michael J. Umholtz

Follow this and additional works at: https://scholar.afit.edu/etd

 Part of the Aerodynamics and Fluid Mechanics Commons

## Recommended Citation

Umholtz, Michael J., "A Comparison of Film Cooling Techniques in a High Speed, True Scale, Fully Cooled Turbine Vane Ring" (2007). *Theses and Dissertations*. 2952.
https://scholar.afit.edu/etd/2952

This Thesis is brought to you for free and open access by the Student Graduate Works at AFIT Scholar. It has been accepted for inclusion in Theses and Dissertations by an authorized administrator of AFIT Scholar. For more information, please contact AFIT.ENWL.Repository@us.af.mil.

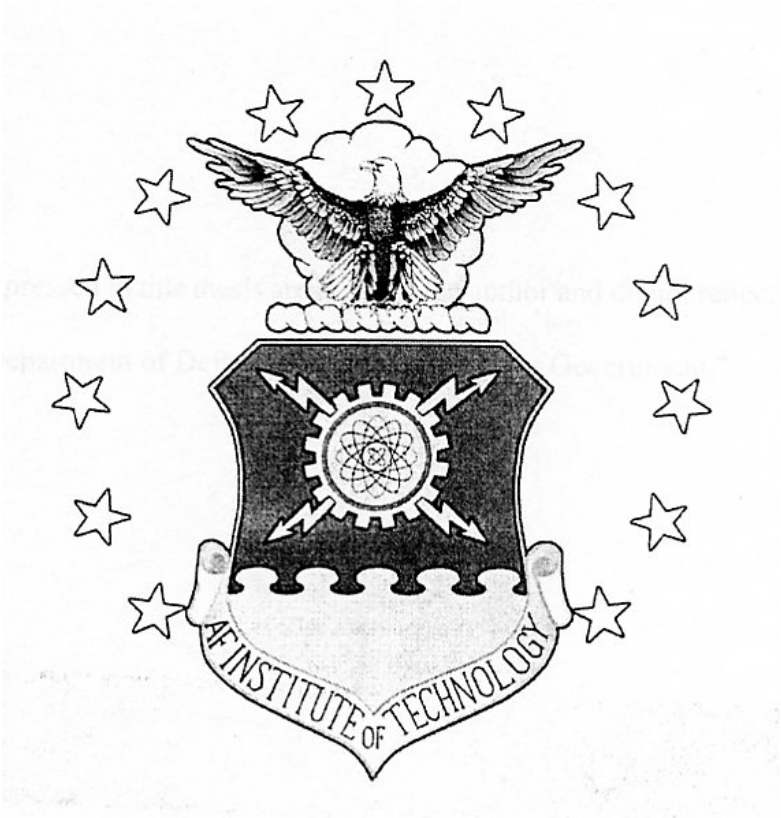


**A COMPARISON OF FILM COOLING TECHNIQUES IN A HIGH SPEED, TRUE SCALE, FULLY COOLED TURBINE VANE RING**

THESIS

Michael Joseph Umholtz, Ensign, USN

AFIT/GAE/ENY/07-J21

**DEPARTMENT OF THE AIR FORCE**
**AIR UNIVERSITY**

**AIR FORCE INSTITUTE OF TECHNOLOGY**

**Wright-Patterson Air Force Base, Ohio**

APPROVED FOR PUBLIC RELEASE; DISTRUBUTION UNLIMITED

The views expressed in this thesis are those of the author and do not reflect the official policy or position of the United States Navy, United States Air Force, Department of Defense, or the United States Government.

AFIT/GAE/ENY/07-J21

# A COMPARISON OF FILM COOLING TECHNIQUES IN A HIGH SPEED, TRUE SCALE, FULLY COOLED TURBINE VANE RING

THESIS

Presented to the Faculty

Department of Aeronautics and Astronautics

Graduate School of Engineering and Management

Air Force Institute of Technology

Air University

Air Education and Training Command

In Partial Fulfillment of the Requirements for the

Degree of Master of Science in Aeronautical Engineering

Michael J Umholtz

Ensign, USN

June 2007

APPROVED FOR PUBLIC RELEASE; DISTRUBUTION UNLIMITED

AFIT/GAE/ENY/07-J21

# A COMPARISON OF FILM COOLING TECHNIQUES IN A HIGH SPEED, TRUE SCALE, FULLY COOLED TURBINE VANE RING

Michael J. Umholtz
Ensign, USN

Approved:

_____/signed/_____ _____
Dr. Mark Reeder Date

_____/signed/_____ _____
Dr. Paul King Date

## Abstract

An effort was undertaken to understand the impact of different film cooling configurations in a true scale turbine vane for three proprietary airfoil designs. The measurements for this study were taken at the United States Air Force Turbine Research Facility (TRF). The TRF enabled heat transfer data to be obtained on full scale turbine hardware under realistic engine conditions. The surface heat flux of the turbine blades was analyzed using the impulse response method. The overall effectiveness was compared between airfoil types at 60% span over varying streamwise locations on both suction and pressure surfaces. Using an approximated massflow, a comparison of the overall effectiveness with respect to massflow rate could be made between airfoils at three different airfoil locations. The shaped hole and slot cooling configurations were found to have higher average overall effectiveness for lower massflow rates than the multiple hole configuration based on the conditions tested.

*For my family and friends*

## Acknowledgements

I would like to thank the team at the Turbine Research Facility for performing these experiments and ensuring quality results: Michael Kobelak for his help in running the experiments, Terry Gillaugh for setting up the film cooling hardware, John Finnegan for making sure the data channels were working, Robert Free for installing the heat flux gauges and thermocouples, Brett Miller for helping me learn the computer system, Rich Anthony for helping me understand the heat flux code, and Michael Barringer for his work with the uncooled vane.

Table of Contents

Page

## List of Figures

Figure Page

Page

## List of Tables

Table Page

# I. Introduction and Background

## *Gas Turbine Film Cooling*

Gas turbine engines have become an integral part of our society as we use them to propel our aircraft and naval vessels as well as generate electricity. Ever since Frank Whittle first applied for a patent on his turbojet engine in 1929, turbine engines have been advancing to meet the needs of our technological world. One way to increase the performance of gas turbine engines is to increase the temperature of the gas as it enters the turbine section; thus we find that durability, thermal efficiency, and output are a function of the turbine rotor inlet temperature. Turbines must therefore be designed to withstand these high temperatures repeatedly over their work cycle.

A method for keeping turbine blades cool has been developed that utilizes high-pressure bleed air from the compressor that is exhausted into internal passages and exits through small holes machined into the airfoil surface. This cooler bleed air will then cover the airfoil surface, forming a film that will shield the metal from the oncoming hot gas from the combustor. This technique is known as film cooling, and allows the gas temperatures entering the turbine to be higher than could normally be withstood by the airfoil metal.

Military gas turbine engines can now have turbine inlet temperatures of over 1600°C, which can be achieved using 20-30% of the total flow to cool the turbine airfoils (Bogard and Thole, 2005:1). Therefore, it is clear that film cooling is an important technology in the performance of gas turbine engines. Effective film cooling reduces the

airfoil surface temperature while using as small of an amount of compressor bleed air as possible so as not to degrade the overall performance of the engine. It is therefore imperative to design film techniques to meet this objective. The one major advancement in this technology is the incorporation of exit shaping to the film holes to result in lower momentum coolant injection jets with greater surface coverage (Bunker, 2005:1). Traditionally this has been accomplished with rows of small cylindrical holes oriented at different angles relative to the airfoil surface. Manufacturers have since developed different techniques and new hole geometries, such as fan shaped holes, slots and multiple holes to improve the effectiveness of film cooling. The target for shaped film holes is to expand the exit area in the plane of the surface of the injection jet by a factor of two to three times that of the round jet without separation. This diffusion of the injected flow can lead to lower blowing ratios, lower aerodynamic mixing losses, and greater lateral coolant coverage, thus increasing cooling effectiveness and efficiency (Bunker, 2005: 2). Figure 1 shows a simple schematic of a film cooled turbine airfoil. The coolant bleed air is fed to the holes on the airfoil surface via entrances on the inner and outer diameters of the airfoil.

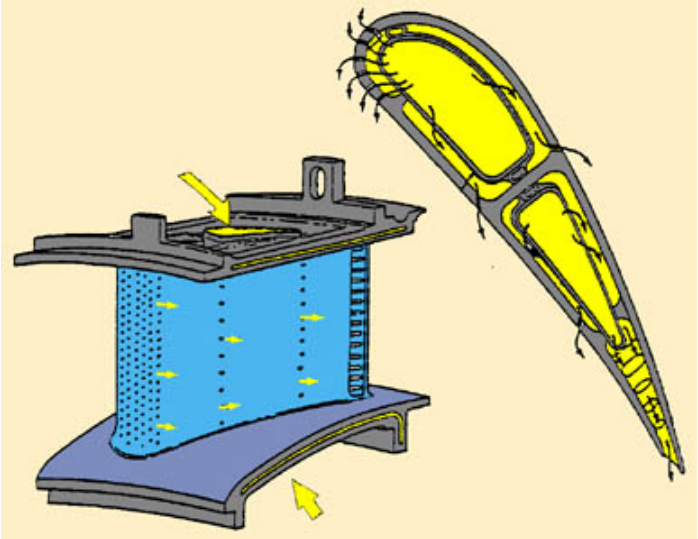

**Figure 1: Film cooled turbine airfoil**

## *Film Cooling Analysis*

An accurate and thorough analysis is required to ascertain how useful a particular film cooling technique is. It must be remembered that the overall goal of using film cooling is to reduce the working temperatures of the airfoils and thus extend the life of the turbine components. This is accomplished by decreasing the local fluid temperature near the airfoil surface. The heat transfer rate from the air to the metal is modeled by the equation:

$$q'' = h(T_f - T_w) \tag{1}$$

Where $h$ is the convective heat transfer coefficient with film cooling, and $T_f$ is the fluid temperature above the surface, both of which vary widely over the airfoil surface (Bogard and Thole, 2005: 2).

Manufacturing film cooled turbines is costly, thus it is important to determine if a particular film cooling configuration improves the performance or not. What needs to be found is the net heat flux reduction, which is defined by the formula:

$$\Delta q = 1 - (q''_{cooled} / q''_{uncooled}) \quad (2)$$

The net reduction relates the heat transfer rate of a film cooled surface to that of a surface with no film cooling.

The heat transfer coefficient and film cooling effectiveness are desired. The film cooling effectiveness is defined as:

$$\eta = (T_\infty - T_{aw}) / (T_\infty - T_{coolant}) \quad (3)$$

Where $T_\infty$ and $T_{aw}$ are the freestream and adiabatic wall temperatures, respectively. Traditionally, the effectiveness is solved by performing two separate tests, one where the coolant temperature is matched to the freestream and a heater surface is used to measure the heat transfer coefficient, and a second experiment where the airfoil surface is made of a low conductivity material to reduce the heat transfer (Sen, Schmidt, and Bogard, 1996). However, real turbine airfoils do not have adiabatic surfaces, so this method will not provide accurate results when measuring temperatures on real engines under real conditions. While tests can be run with the coolant temperature matched to the inlet freestream value, the use of heater foils is not practical. Thus the values of the heat transfer coefficient and the film effectiveness are difficult to determine. The driving temperature is a mixture of the local freestream and coolant flow which is difficult to measure and quantify.

For this study the surface temperature of the turbine airfoils was quantified in terms of the overall effectiveness, which is defined as

$$\phi = \frac{T_\infty - T_w}{T_\infty - T_c} \quad (4)$$

Since actual airfoil surface temperatures are not often known in laboratory experiments, a constant value of 0.6 is often assumed (Mouzon, Albert, Terrell, Bogard, 2005: 2). However, for this study surface temperatures have been measured subject to the true operational environment, so exact values of the overall effectiveness will be presented. A comparison of each film cooling technique will be based on the heat flux and the overall effectiveness rather than on the heat transfer coefficient and adiabatic effectiveness as is traditionally done.

The design of film cooled turbine airfoils involves the prediction of the effectiveness distribution downstream of the coolant holes (Bogard and Thole, 2005:3). However, there are many factors and operating conditions that affect the heat transfer in film cooled turbines. These include the mass flow, geometry and configuration of the coolant exit holes, turbulence, and surface roughness.

# II. Literature Review

## *Mass Flow Effects*

The coolant mass flux ratio or blowing ratio is defined as the ratio of the density and velocity of the coolant flow to that of the mainstream flow:

$$M = (\rho U)_c \Big/ (\rho U)_\infty \tag{5}$$

At high blowing ratios, the coolant jets have a tendency of separating from the airfoil surface at the hole exit. This separation results in a large decrease in film effectiveness at high blowing ratios (Bogard and Thole, 2005: 4), (Schulz, 2001: 143). In a study of patterns of film effectiveness based on lift off and mixing phenomena, it was found that at low blowing ratios, a fully attached coolant jet was observed, and that counter rotating vortices of the coolant flow were near the surface, enhancing heat undesirable transfer (Schulz, 2001: 142). It has also been found that the adiabatic effectiveness is primarily a function of the blowing ratio, the width and height of the injection hole, and the downstream distance (Kays and Crawford, 1987: 297).

## *Hole Geometry and Configuration*

The hole exit geometries analyzed in this study were fan shaped holes, slots, and multiple, discrete cylindrical holes. Besides the shape of the hole exit, several other geometric parameters affect film cooling. These include pitch-to-diameter ratio, length-

to-diameter ratio, and orientation of the hole with respect to the freestream flow (Sen, Schmidt, and Bogard, 1994: 1).

The surface angle of the cooling holes may be oriented with the freestream flow direction or inclined with respect to the freestream. Coolant holes that are directed at a nonzero angle from the freestream direction are called compound angle holes. A study by Schmidt et al revealed that film cooling with compound angle injection does not provide higher adiabatic effectiveness at the optimum momentum flux ratio, but does provide high effectiveness over a larger range of momentum flux ratios (Schmidt, Sen and Bogard, 1994: 813).

Another important geometric parameter in film cooling is the spacing or pitch between holes. Cooling holes are typically spaced apart at about three hole diameters, but can range up to eight hole diameters in some cases (Bogard and Thole, 2005: 7). In a study performed by Dittmar et al, on a model of a suction side of an actual turbine guide vane assembled in an open loop atmospheric wind tunnel, the cooling performance of a single row of 8 fan-shaped holes was compared to a double row arrangement of 16 cylindrical holes. The fan shaped holes were spaced apart at four cylindrical-hole diameters. The cylindrical holes were also spaced apart at four diameters and the second row of holes was staggered from the first by a distance of two diameters. Their results found that a double row of cylindrical holes provided nearly similar adiabatic film cooling effectiveness values compared to a single row of fan-shaped holes only at small blowing ratios ($M<1$), and that at medium and high blowing ratios the fan-shaped holes had a much better cooling effectiveness (Dittmar, Jung, Schulz, Wittig, and Lee, 2001: 321-328).

In a study performed by Sargison et al, the heat transfer coefficient and adiabatic effectiveness of cylindrical, fan-shaped holes and a slot were compared in a steady state, low speed facility at engine representative Reynolds number. It was found that the fan-shaped hole showed an improvement in the uniformity of downstream cooling as well as an improved lateral film cooling effectiveness when compared to discrete, cylindrical holes. It was also found that the slot had a better film effectiveness than the fan shaped hole; however, both the cylindrical and fan-shaped holes had a lower heat transfer coefficient than the slot. They concluded that the drawback of the fan-shaped holes was that the aerodynamic loss was significantly higher than both the slot and discrete cylindrical hole values due to poor diffusion at the hole exit expansion (Sargison, Guo, Oldfield, and Rawlinson, 2001: 367-368). It was also found that the two dimensional flow of coolant from the slot is devoid of the vortex formation and thus has a higher film cooling effectiveness both upstream and downstream of the slot exit (Sargison, Guo, Oldfield and Rawlinson, 2001: 362).

A study performed by Bunker explored the film cooling adiabatic effectiveness for a traverse slot fed by a row of discrete, angled cylindrical holes on a flat plate inside a wind tunnel at a range of blowing ratios from 0.75 to 4. His study found that the film cooling effectiveness was not affected much by the blowing ratio over the range of one to four. This would imply that the same film effectiveness could be achieved for low coolant flow as for higher flow, resulting in savings in coolant for specific applications (Bunker, 2002: 9). It was also reported that the ideal film cooling scheme is a tangentially injected two-dimensional layer of coolant on the airfoil surface, from which adiabatic effectiveness levels can approach unity at the coolant injection point (Bunker,

2002: 1). According to that study, the discrete holes-in-slot geometry can achieve film effectiveness values close to the ideal two-dimensional slot, but only upon sufficient development of the lateral flow within the slot.

A study performed by Gritsch et al, presented measurements of the film cooling effectiveness for a cylindrical hole, a fan-shaped hole, and a laidback fan-shaped hole. The measurements were conducted in a continuous flow wind tunnel, with the air supply provided by a high pressure, high temperature test facility (Gritsch, Schulz, and Wittig, 1997: 2). The study concluded that the expanded, fan-shaped holes displayed significant improvement in thermal protection of the airfoil surface downstream of the ejection location, particularly at high blowing ratios, as compared to the cylindrical holes. The laidback fan-shaped holes also provided better lateral spreading of the coolant jet then the fan-shaped holes and cylindrical holes, thus providing increased laterally averaged effectiveness (Gritsch, Schulz, and Wittig, 1997: 1,9).

Sweeney and Rhodes analyzed a flat plate specimen undergoing film cooling with multiple cylindrical holes using infrared imaging. Their research was done for a turbine manufacturer; with results presented in terms of the overall effectiveness. It was found that improvement in the effectiveness was most apparent on closely spaced holes due to the development of full film coverage on the hot surface. They concluded that the overall effectiveness is an appropriate measure of cooling performance for internal impingement, through-the-wall conduction, and full-coverage film cooling (Sweeney and Rhodes, 2000: 171). Their results show the influence of freestream Reynolds number on overall effectiveness and the convective heat flux to the airfoil surfaces. They found that the overall effectiveness decreased as the Reynolds number varied from $1.0 \times 10^6$ to $1.8 \times 10^6$

for varying coolant mass flow in the case of a multiple hole airfoil (Sweeney and Rhodes, 2000: 175). Their results also show the importance of the overall effectiveness to turbine airfoil designers, as it is a more feasible measurement of film cooling performance in real turbine hardware.

## *Turbulence Effects*

Film cooling analysis is also affected by the freestream turbulence. Turbulence is quantified by the equation:

$$Tu = u_{rms} / U \tag{6}$$

This is defined as the rms levels of the velocity fluctuations divided by the magnitude of the mean velocity. It has been found that high freestream turbulence can prevent coolant jets from detaching from the airfoil surface (Bogard and Thole, 2005: 12).

In a study done by Suslov et al, the impact of unsteady flow and turbulence on heat transfer was observed. Unsteady flow results when film cooling jets experience a variation in the mainstream flow as the blades through the wakes of the upstream vanes (Bogard and Thole, 2005: 12-13). These wakes are characterized by their high turbulence intensity, and were found to have a strong impact on the heat transfer on the suction side of the blades (Suslov, Schulz, and Wittig, 2001: 255). It was also found that the laminar-turbulent transition increases the likelihood that the boundary layer will remain attached and thus can prevent the coolant jet from separating from the surface (Suslov, Schulz, and Wittig, 2001: 256).

In the study performed by Dittmar et al discussed previously, a comparison of the film cooling effectiveness between cylindrical holes and fan-shaped holes was performed at freestream turbulence values of *Tu=6%* and *10%* (Dittmar, Jung, Schulz, Wittig, and Lee, 2001: 321). It was found that enhanced freestream turbulence intensity reduced film cooling effectiveness due to greater rate of convection, and that greater turbulence leads in general to a faster decay of effectiveness downstream of the hole exits (Dittmar, Jung, Schulz, Wittig, and Lee, 2001: 328).

Barthet and Kulisa performed a study on the three-dimensional flow phenomena that is caused by coolant jet injection from shaped and cylindrical holes on a flat wall at a blowing ratio of 0.95. It was found that the increased cross-sectional area of the shaped hole exit leads to a reduction of the mean velocity, and thus the momentum flux of the coolant jet exiting the hole, and therefore the penetration of the jet into the mainstream flow is reduced, resulting in increased cooling efficiency (Barthet and Kulisa, 2001: 370). It was also found from their study that vortex dynamics influence the cooling efficiency of both hole shapes. For the cylindrical holes, it was found that counter-rotating horseshoe vortices are formed at the hole exit resulting from the coolant jet disrupting the mainstream flow. These counter-rotating vortices pull the coolant flow from the surface and consequently push the hot mainstream flow towards the surface, resulting in a decrease of local film effectiveness (Barthet and Kulisa, 2001: 372). For the shaped holes, similar induced vortices were observed, as well as one additional peculiar phenomenon. In this case, the mainstream flow entered the cooling hole and was absorbed by the leading edge vortex, and it was reported that this ingestion reduced the film effectiveness of the coolant jet (Barthet and Kulisa, 2001: 373).

## *Surface Roughness Effects*

A study of film cooling performance on rough surfaces is representative of real turbine hardware that has been worn due to repeated operation. A rougher turbine airfoil surface can lead to increased turbulent mixing in the boundary layer and can often reduce film effectiveness and increase the heat transfer rate (Bogard and Thole, 2005: 13). This increased heat transfer rate is caused by increased eddy convection down to the plane of the roughness elements, this is due to the face that a rough surface yields a sixty percent increase in Stanton number over that of a smooth surface (Kays and Crawford, 1993: 298-300). A study performed by Rutledge et al found that the dominant effect of surface roughness was a doubling of the heat transfer coefficients, and that relative to a film cooled smooth surface, a film cooled rough surface increased the heat flux to the surface by 30-70% (Rutledge, Robertson, and Bogard, 2006).

# III. Experimental Setup

## *Experimental Facility*

The experiment performed for this study was done in the Turbine Research Facility (TRF) at the Air Force Research Laboratory at Wright Patterson Air Force Base in Dayton, Ohio. The TRF is a short duration blow-down facility that can match engine Reynolds number, Mach number, pressure ratio, gas to metal temperature ratio, corrected speed, and corrected mass flow of real turbine hardware (Barringer, Thole, Polanka, 2006:3). A photograph of the TRF test setup can be seen in the figure below.

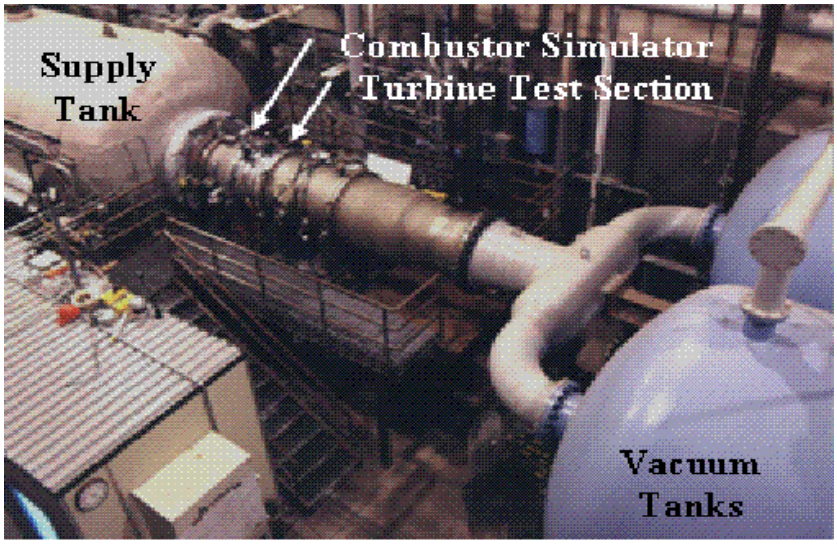


**Figure 2: Photo of TRF facility**

The facility consists of a large supply tank, a turbine test section, and two large vacuum tanks. The test section is a true scale, single turbine stage with vanes and blades.

To perform a test, the supply tank is filled with gas (usually nitrogen) and pressurized and heated to an aerodynamic and thermodynamic match point. An isolation valve acts as a choke for the system and controls the pressure ratio. Once the main valve opens, the blow down process is initiated as well as the data acquisition and traversing system. Flow proceeds through a combustor simulator section which serves to alter the total pressure and temperature profiles of the flow to that which would be found in a real combustor (Barringer, Thole, Polanka, 2006). This combustor simulator creates the initial conditions for the turbine test section. After passing through the test section, the flow proceeds through past the isolation valve into the vacuum tanks.

The system consisted of two secondary blowdown systems wherein cryogenic nitrogen was delivered to the test article. One loop brought the coolant flow to the outside diameter of the rig feeding the vane leading edge and the blade outer air seal. The second loop proceeded to the inside of the facility to supply the vane trailing edge and the rotor. Each loop was fed by a large holding tank installed on either side of the main supply tank shown in Figure 2. The initial conditions were achieved in these tanks by bringing liquid nitrogen into the tank and allowing it to expand to a gas. To achieve the proper initial temperature, a control valve was used to allow more or less nitrogen into the tank. Another control valve was utilized to vent off any excess pressure in the tank and hold the desired test pressure. The filling process was repeated until the conditions were close and then fine-tuned to the desired temperature by the used of heater rods. A fan was used to stir the gas in the tanks in order to obtain uniformity. Once the desired conditions were achieved, fast acting valves were independently set to fire each gas stream. The massflow was measured with the use of a calibrated sonic throat venturi

that contained a needle valve which enabled the throat area to be changed to set the massflow. After passing through the venturi, each line entered a manifold. One manifold split the coolant flow into multiple one-inch lines to feed the outside of the vane case which in turn fed the showerhead region of each airfoil. The other manifold split the coolant flow into two four-inch lines that fed struts on the top and bottom of the rig and then passed through the inside of the facility. This flow served as the coolant for the downstream section of the airfoils. These flow lines were sized as a balance between keeping them large enough to keep the Mach number below 0.2 in the lines to minimize pressure losses and small enough to minimize the flow through time of the flow. All of theses lines and hardware external to the facility are insulated and precooled to about -100°F to reduce the temperature rise through these lines as the test progressed. The precooling was accomplished by injecting a small amount of liquid nitrogen downstream of the fast acting valve and allowing it to expand and traverse through the flow lines to the rig. At the rig a set of three way valves diverted this flow out to vent. Prior to the test initiation the liquid nitrogen was shut off and the diverter valves adjusted to bring the coolant flow into the test article. The internal hardware was initially maintained at room temperature via a set of water jackets.

For each test, tunnel operation and data collection was performed by AFRL/PR personnel. A total of 23 runs were conducted for this test matrix, and for this study runs 2, 10, 12 and 21 were analyzed. There was difficulty in analyzing all of the runs conducted due to errors, likely caused by spurious data points. Values of the overall effectiveness were found for each cooling configuration for the thin film gauges at 60% span, and varying streamwise locations.

## *Experimental Instrumentation*

The film cooled vane consisted of a configuration of three different cooling configurations. While the type of film cooling scheme altered the placement of the cooling holes, all three were designed to keep the same airfoil cool at the same nominal mass flow rate. Each airfoil was individually flow checked to understand what the actual mass flow distribution would be for each test condition. Figure 3 and Figure 4 show the distribution of coolant massflow to each airfoil type based on the inner and outer diameter feed lines. There are two multiple hole and slot airfoils used because a different airfoil was used in analyzing either the suction surface or pressure surface in this study.

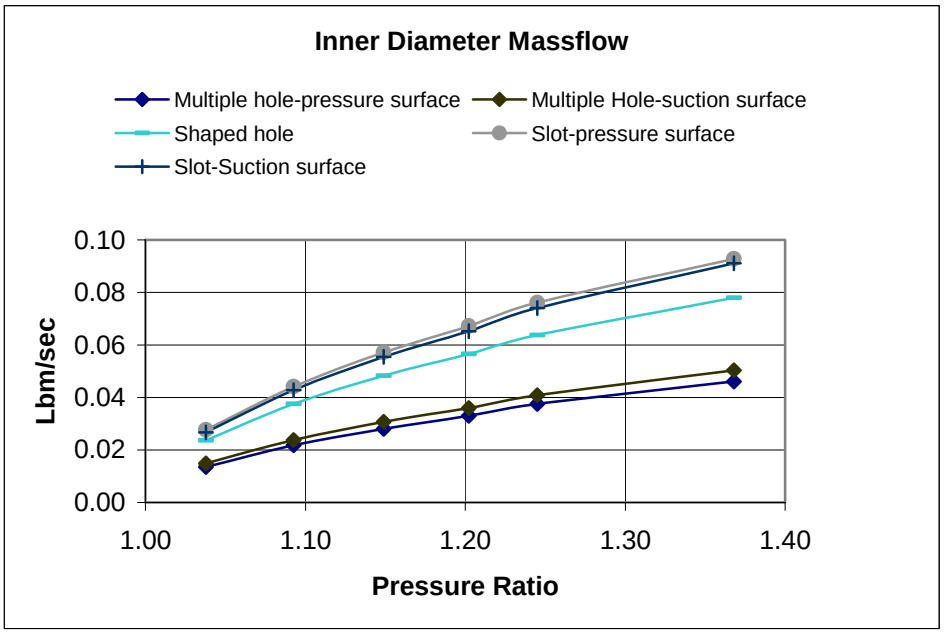


**Figure 3: Inner diameter massflow with respect to pressure ratio for each airfoil type.**

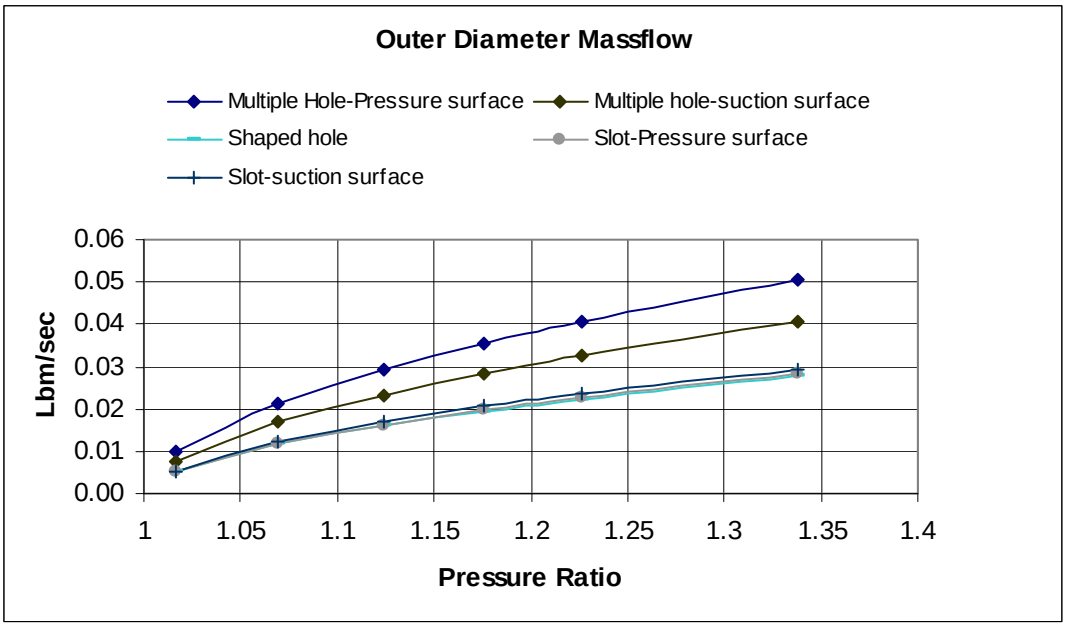


**Figure 4: Outer diameter massflow with respect to pressure ratio for each airfoil type.**

The vane utilized different transducers to obtain readings of pressure and temperature during each run. There were two arrays of Kulite pressure transducers at nominally 60% and 90% span, with 5 on the pressure side and 7 on the suction side of the airfoils. In this study, the heat transfer gauges were analyzed at the 60% span location and varying streamwise locations.

The heat flux gauges consist of a thin film platinum gage sputtered onto a Kapton substrate and are mounted on top of 3-mil, E-Type thermocouples that were embedded into the airfoil surface. The thermocouples were installed such that the tip of the thermocouple just slightly extends (less than 1-mil) from the surface of the airfoil and thus makes good thermal contact with the back side of the Kapton heat flux gauge and is at a known position. This exact placement of the thermocouple to the heat flux gauge is important for properly calculating heat flux based on the double-sided impulse response

method, as will be discussed later. The gauge and thermocouple pairs used were located at the following streamwise locations: for the shaped hole airfoil, 17.1%, 57.3%, and 75.2% surface length on the suction side, and for the multiple hole airfoil, -80.2%, -51.4%, -22.8% surface length on the pressure side, 14.7% and 65.4% surface length on the suction side. These distances were measure from the leading edge of the airfoil, and the convention of positive percent surface length applies to the suction side while negative percent surface length applies to the pressure side. Upstream temperature was measured using a temperature rake containing thermocouple beads. Data was acquired at a rate of 20 kHz.

The heat transfer gauges used in this experiment are high-density gauge arrays in which voltage fluctuations are measured across a thin film resistance supplied with a constant current (Anthony, Jones, Oldfield, LaGraff, 1999: 3). An external current source is maintained constant through all the gauges, and the differential voltage drop across each gauge is measured. These gauges are capable of high frequency, high spatial resolution measurements in rapid and turbulent surface heat transfer experiments (Anthony, Jones, Oldfield, LaGraff, 1999: 7).

## *Data Analysis*

The data collected in this experiment had to be analyzed properly to obtain the necessary results. A technique described below was needed to find the heat flux into the surface of the airfoils, and measurements of the freestream, coolant, and surface temperatures were needed to find the overall effectiveness.

## Heat Flux Measurement

Dr. Martin Oldfield of the University of Oxford has developed a new, computationally efficient method for processing transient thin-film heat transfer gauge signals (Oldfield, 2006:1). The method utilizes the discrete impulse response for particular heat transfer gage configurations. The common configuration is the semi-infinite substrate model; however the airfoils used in this experiment have thin walls and are not semi-infinite, therefore this experiment utilized the double-sided heat flux gauge method. The advantage of this model is that the heat transfer rate can be found in configurations where the semi-infinite assumption does not hold. The disadvantage is that two temperatures must now be measured instead of just one, thus increasing the resultant uncertainty.

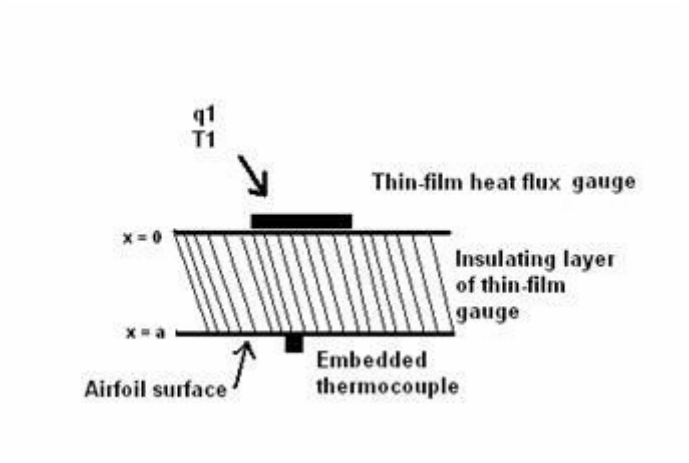


**Figure 5: The double-sided, thin film heat flux gage model.**

The impulse response method uses discrete deconvolution to derive filter impulse responses of the same length as the data being processed from analytically derived

response functions (Oldfield, 2006:2). The time varying heat flux can be found based on the equation:

$$q(t) = h(t) * T(t) = \int_{-\infty}^{\infty} h(\tau) T(t-\tau) d\tau \tag{7}$$

Where h is the impulse-response function, T is the temperature function and the (*) is the convolution operator. The convolution can be carried out in *Matlab*, with *h* being dependent on the material properties and sampling frequency. The impulse response need only be derived once for each gauge for a given sampling rate, and can be reused repeatedly using *Matlab* (Oldfield, 2006:1). A detailed derivation of the impulse response method can be found in appendix I.

The top surface heat transfer rate $q$ into a double sided thin film heat transfer gauge with top temperature $T_1$ and bottom temperature $T_2$ can be considered to be the superposition of two situations: Differential heat transfer $q_d$ with $(T_1-T_2)/2$ applied to the top and $-(T_1-T_2)/2$ applied to the bottom, and thus with zero temperature change with time in the middle. Common mode heat transfer $q_c$ with $(T_1+T_2)/2$ applied to the top and $(T_1+T_2)/2$ applied to the bottom, and thus with zero heat transfer in the middle. Solutions are found for $(T_1-T_2)/2$ and $(T_1+T_2)/2$ for the case where $q_s$ is a unit step. The first *np* points of the $(T1-T2)/2$ to $q_d$ and $(T1+T2)/2$ to $q_c$ impulse responses are obtained by deconvoluting the known step $q$ and $T$ pairs in sampled form, using the *Matlab* filter function. In z-transform form, the process is $Q(z) = H(z)T(z)$, where $H(z)$ is the z transform of the impulse response $h(t)$. Then, for a known pair of $Q_1(z)$ and $T_1(z)$ sequences, $H(z) = Q_1(z)/T_1(z)$. This can be evaluated by the *Matlab* function *h = filter* $(q_1, T_1, imp)$, where *imp* is the discrete impulse sequence [1 0 0 0 ....]'. In this case we get

two impulse responses: differential $h_d$ from $(T_1-T_2)/2$ and common mode $h_c$ from $(T_1+T_2)/2$. These are then recombined to give the output impulse responses as row vectors: the top surface $h_1 = (h_d + h_c)/2$ and the bottom surface $h_2 = (h_d - h_c)/2$. After the impulse responses $h_1$ and $h_2$ are obtained by this program and stored as a row vectors, they can be used efficiently to compute surface heat flux from a measured sampled $T_1$ and $T_2$ signals. A fast Fourier transform based method is used to filter the temperature and impulse response pairs and give the resultant heat flux vector (Doorly and Oldfield, 1986: 1159-1167).

$$q = fftfilt\ (h_1,T_1) + fftfilt\ (h_2,T_2) \tag{9}$$

The accuracy of the impulse response method depends on the accuracy of the input thermal (material) properties of the gauge and vane surface. These input thermal properties include the density, specific heat capacity and thermal conductivity, or ρ, c and k respectively. The thermal product of these properties $\sqrt{\rho ck}$ is then found, along with the effective thickness, $a/k$ where $a$ is the thickness of the insulating layer. The impulse response can then be found as a function of these properties and the sampling rate.

Once the impulse function is found, it can be used to find the heat flux for all pairs of thin film gauges and thermocouples in which the time varying temperatures are known. To minimize large fluctuations in the heat flux readings, the gauge and thermocouple temperature data were filtered. For this study, a low-pass Butterworth filter was utilized. The filter was designed with a passband corner or cutoff frequency of 0.001 radians per sample, and a stopband corner frequency of 0.01 radians per sample. The maximum permissible passband loss, or ripple was 0.01 decibels, and the stopband

attenuation was 10 decibels. The resulting low-pass Butterworth filter transmits low-frequency signals and attenuates high-frequency signals and sacrifices roll off steepness for monotonic or smooth data distribution. The resulting signal is devoid of high fluctuations between data points while minimizing aliasing (Dally, Riley, and McConnell, 1993: 191). Figure 6 and Figure 7 show the unfiltered and filtered temperature traces respectively. Figure 8 shows a comparison between the resulting heat flux when the temperatures are filtered or not. It can be seen that filtering the temperatures prior to calculating the heat flux will provide an estimate of the average value and clean up the data plot. Some large fluctuations in the heat flux signal are due to the real phenomena of rotor blade passing, but again low pass filtering of the temperature traces will also alleviate high noise levels in the heat flux. It should be noted that for the figures below, the time window between 1 to 4 seconds represents when the actual run begins and ends, respectively. The time windows before and after this window show highly transient behavior due to the opening and closing of the main flow valve. The near constant value in the heat flux during the steady portion of the run shows that the heat transfer mechanism is constant in time once established.

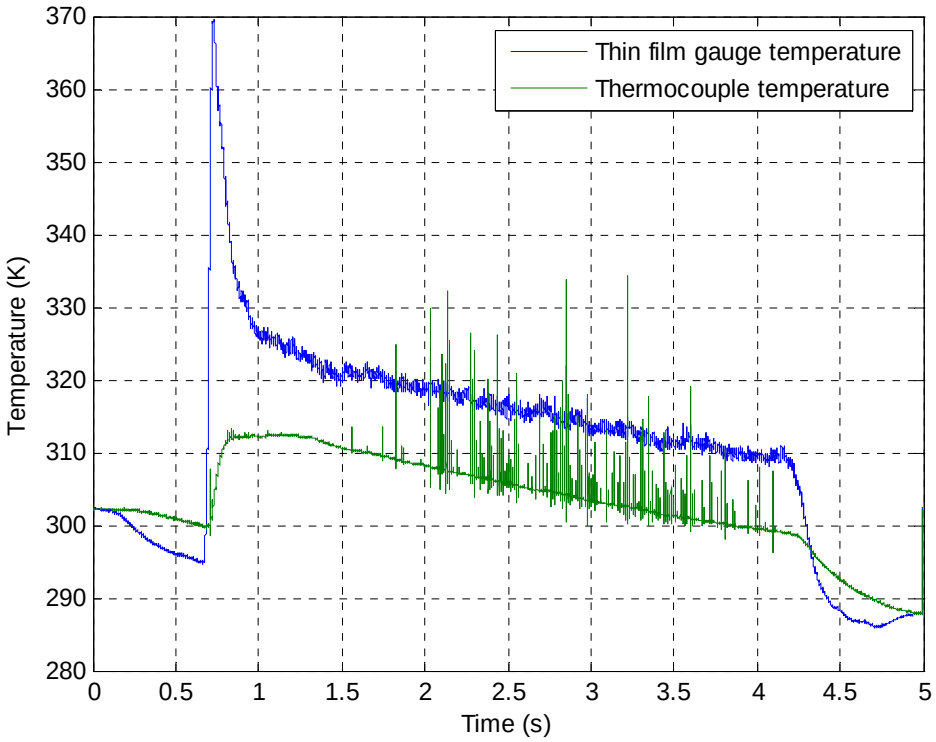


**Figure 6: An example of the unfiltered temperature traces**

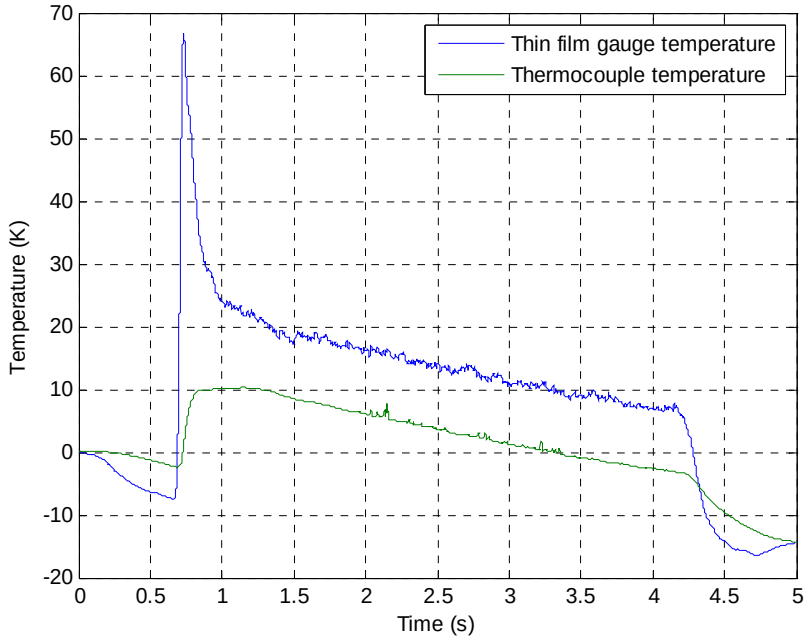


**Figure 7: An example of the filtered temperature traces**

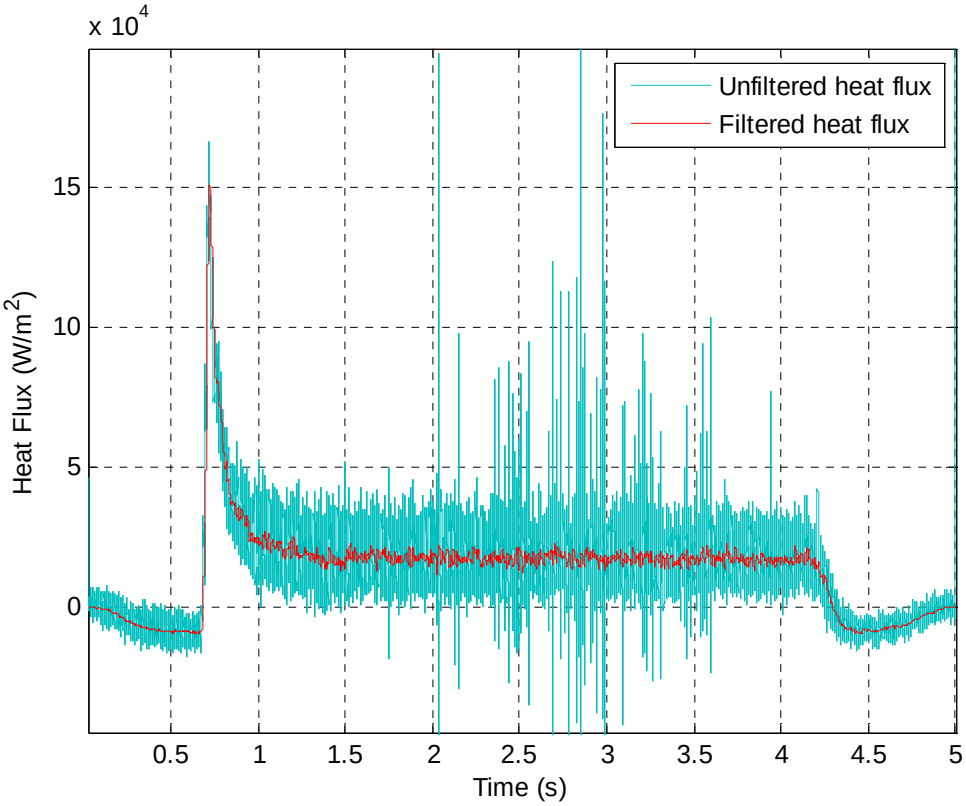


**Figure 8: A comparison of heat flux signals with and without filtering.**

# IV. Experimental Results and Analysis

The main focus of this study was the comparison of three popular film cooling techniques being used in gas turbine engines. Since a reduced surface temperature is the ultimate goal of film cooling, the comparison would be based on the heat flux and overall effectiveness of each of the configurations for varying freestream and coolant flow conditions. A correlation could then be made between the heat flux and effectiveness to different airfoil positions, and an evaluation of the performance could be made.

## *Thermocouple Superposition*

Part of this study explored the possibility of using the impulse response method to find the heat flux between a thin film heat transfer gauge and thermocouple that was not precisely below it. The reason this was studied was to discover if the airfoil surface temperature was uniform enough as to allow a thermocouple that was not directly underneath a thin film gauge to be used to find the heat flux with reasonable accuracy. Figure 9 shows the temperature traces of a thin film gauge and thermocouple that are located at 17.1% surface length on a shaped hole airfoil. Figure 10 shows the temperature traces of a thin film gauge at 17.1 % surface length and a thermocouple at 57.3% surface length. Figure 11 shows the difference in the resultant heat flux that results when these two different temperature traces are used. It is important to note in the figures that the run begins when the temperatures are steady, or between about 1 to 4.2

seconds in these figures, and that the high fluctuations in readings at the beginning and end of the runs are due to the main valve opening and closing respectively.

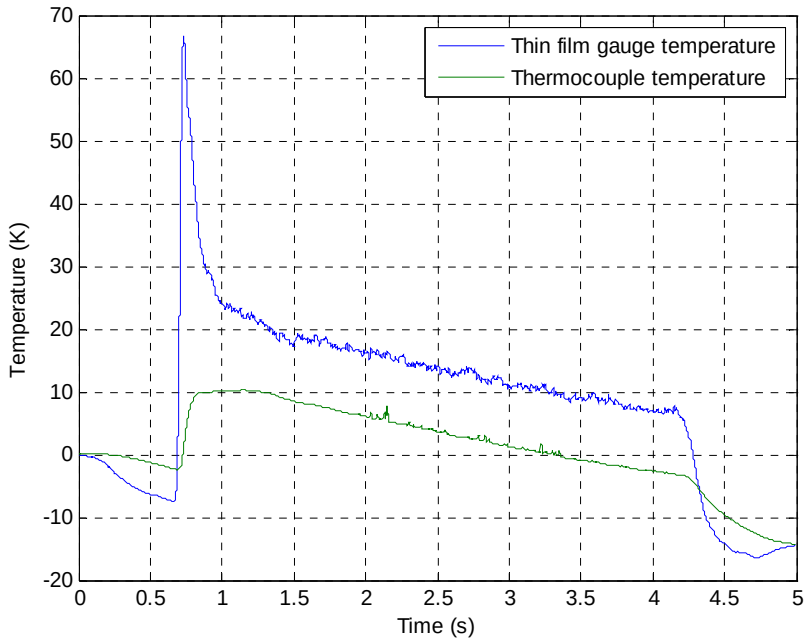


**Figure 9: Thin film and underlying thermocouple temperatures**

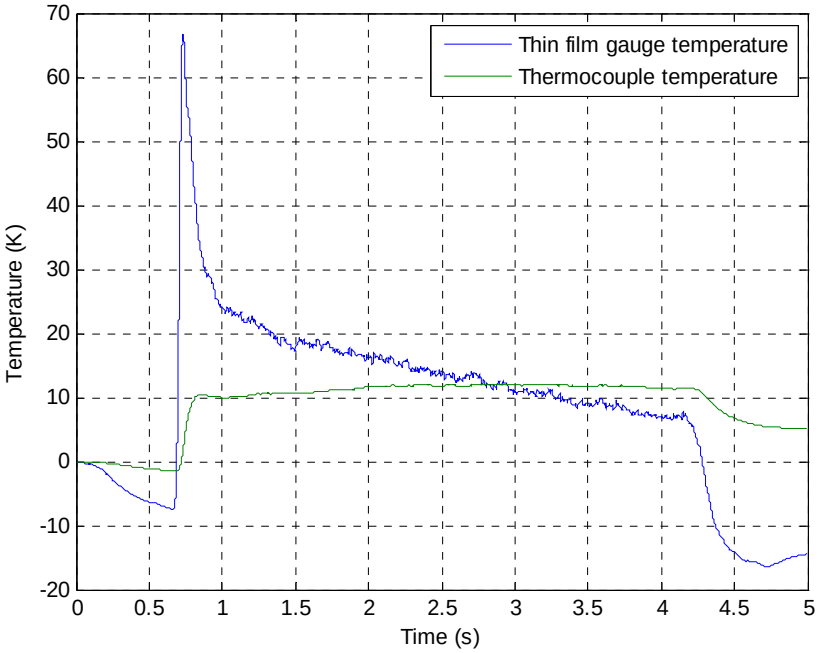


**Figure 10: Thin film gauge at 17.1% surface length and thermocouple at 57.3% surface length.**

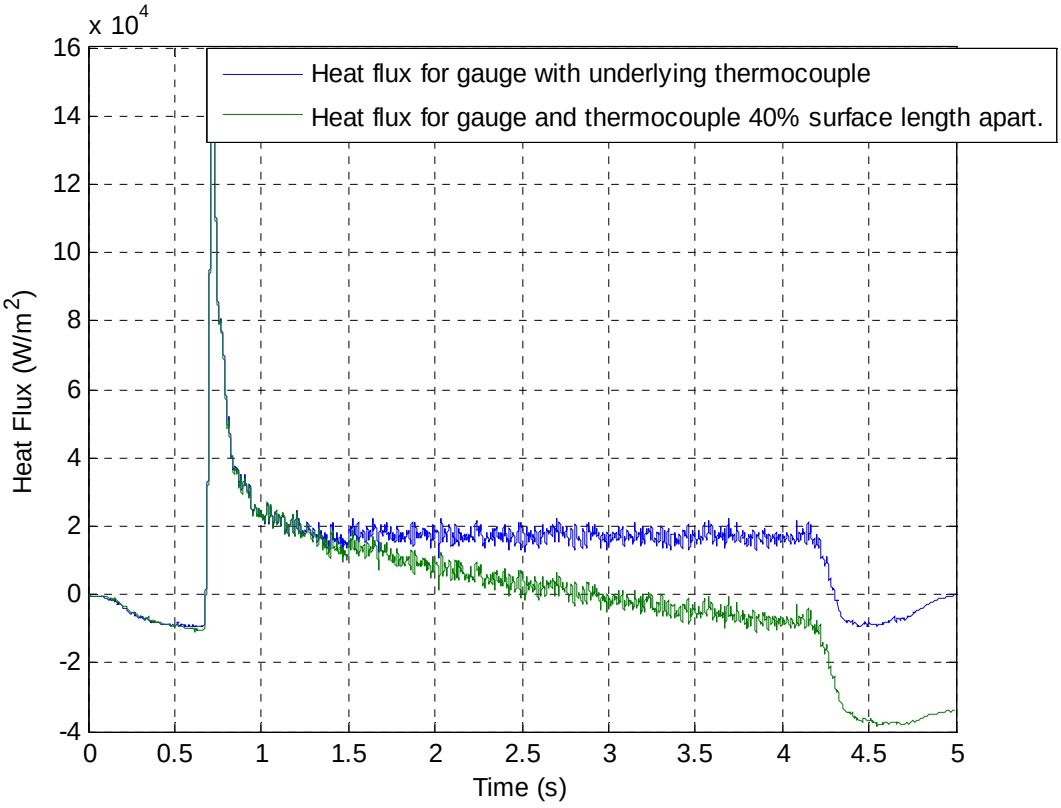


**Figure 11: A comparison in the heat flux.**

From Figure 11 it is apparent that there is a significant difference in the heat flux that results when using different thermocouple with the same gauge. Figure 12 shows how significant this difference can be; ranging in a difference of measurement from -10000 to 9000 W/m$^2$. This is a large difference in heat flux over a distance of less than three inches and clearly this shows that the separation is too large to yield good heat transfer data.

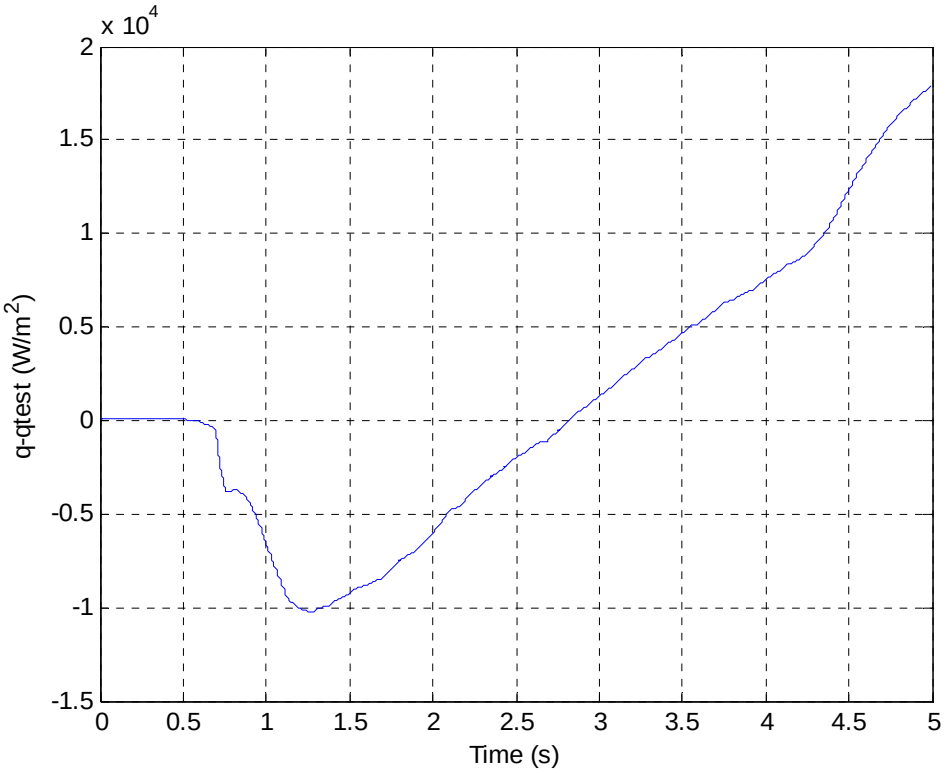


**Figure 12: Error in heat flux using a gauge at 17.1% surface length with a thermocouple at 57.3%.**

A similar test was performed using a thermocouple that was located at 75.2% surface length with the same thin film gauge at 17.1% surface length. Figure 13 shows that the difference in heat flux is just as significant as when the thermocouple was 40%

farther from the gauge. In this case the heat flux difference varied between -20000 to -5000 W/m$^2$. Figure 14 shows another heat flux trace for a thin film gauge and thermocouple pair located at 57.3% surface length for the same test conditions previously used. Figure 15 and Figure 16 show the error that results when the thin film gauge and thermocouple are too far apart. The errors are still just as pronounced as in the previous test.

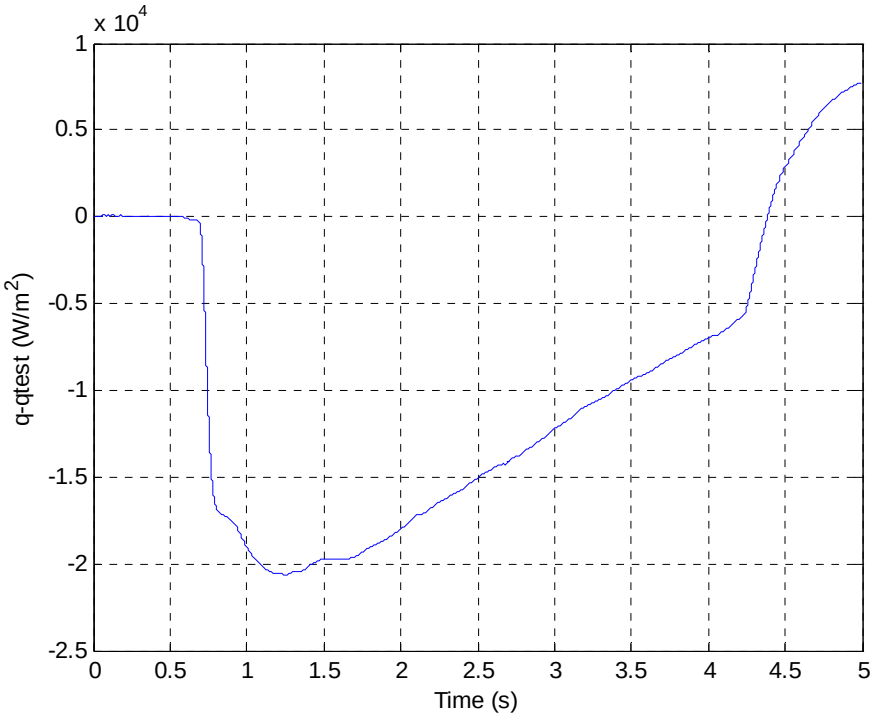


**Figure 13: Error in heat flux using a gauge at 17.1% surface length with a thermocouple at 75.2%.**

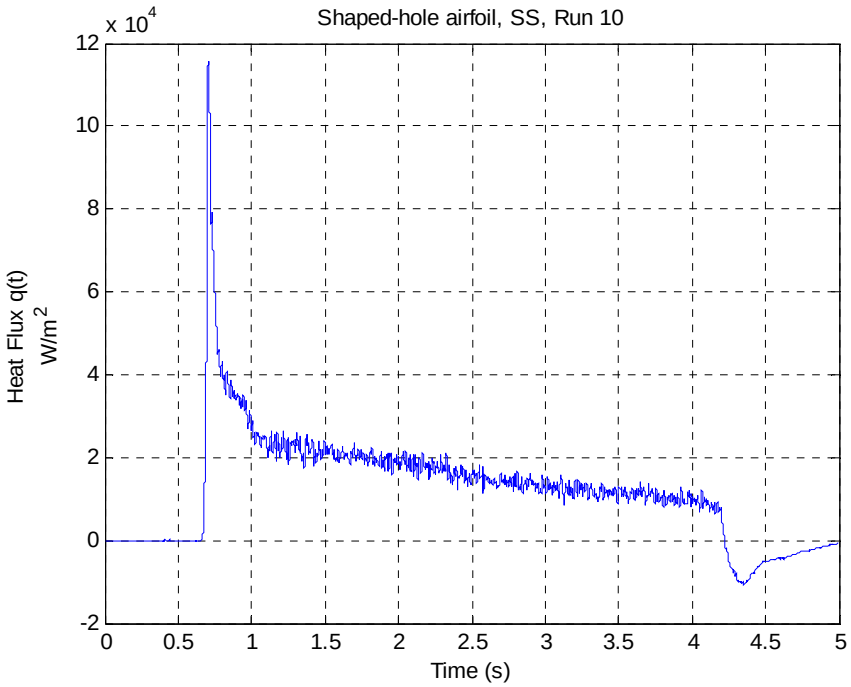


**Figure 14: Heat flux of a thin film gauge and thermocouple pair at 57.3% surface length.**

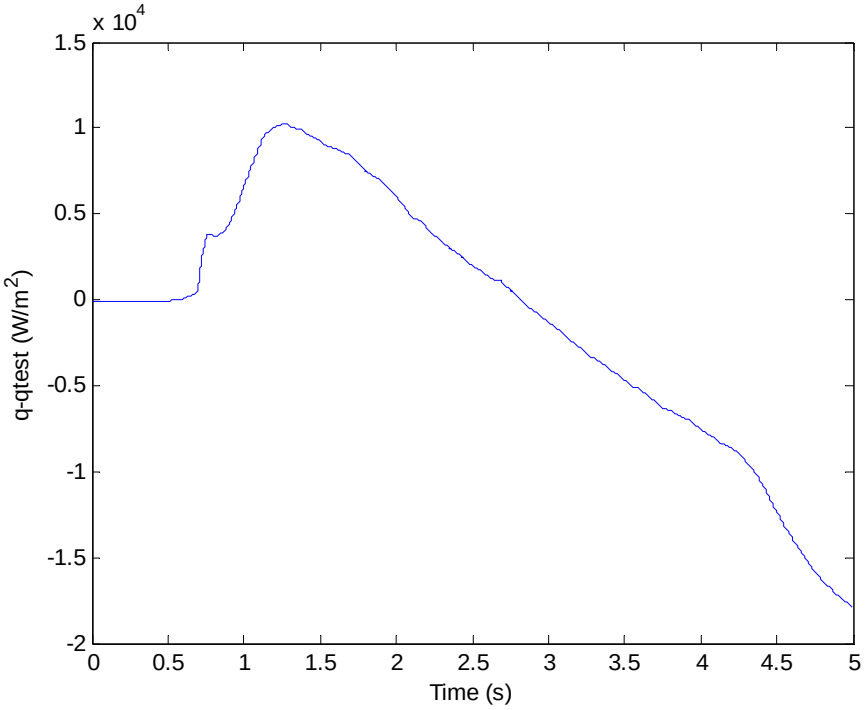


**Figure 15: Error in heat flux using a gauge at 57.3% and thermocouple at 17.1%.**

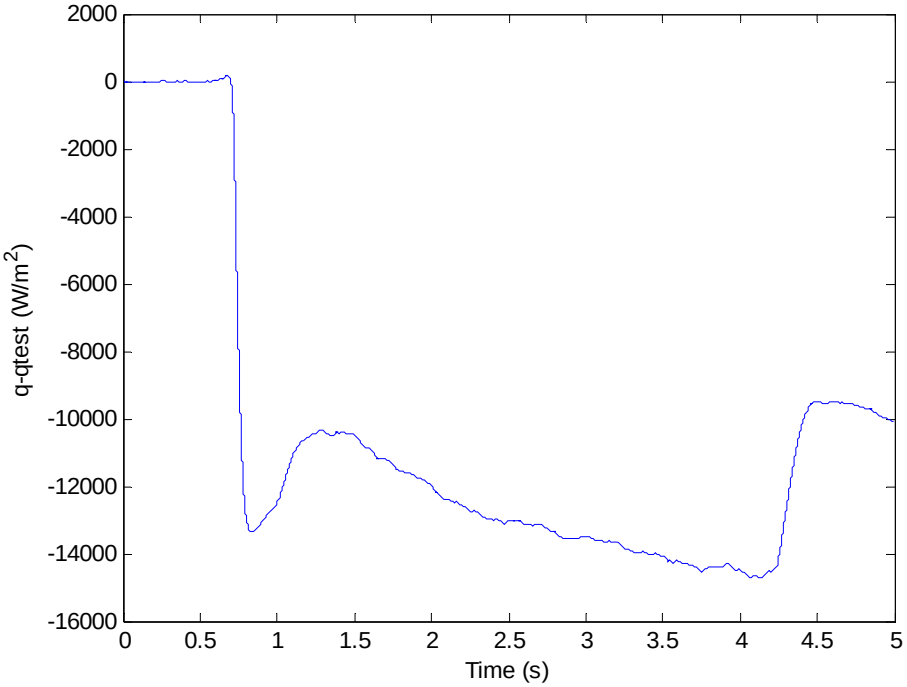


**Figure 16: Error in heat flux using a gauge at 57.3% and thermocouple at 75.2%.**

## *Reynolds Number Effects*

Figure 17 shows the heat flux for a gauge located at 57.3% surface distance along the suction side of the shaped hole airfoil for run 10. By the end of the run, the heat flux has decayed by about 43%. Likewise Figure 18 shows a slight decay of 3.5% in the overall effectiveness for the same gauge. Table 1 shows the decay of the Reynolds number from the beginning of a run to the end and the resulting decay in surface, coolant and freestream temperatures, overall effectiveness and heat flux.

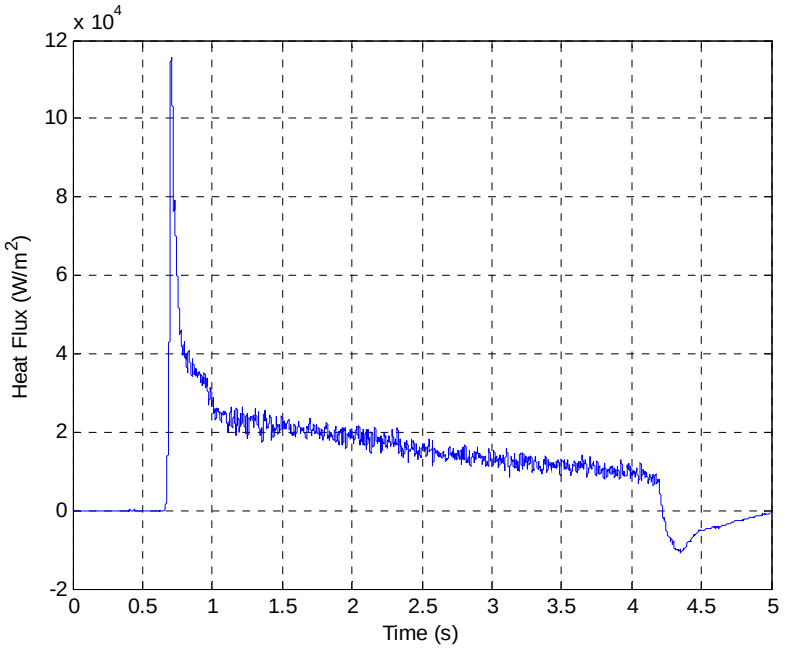


**Figure 17: Heat flux with a decay of 43% between 1 to 4 seconds.**

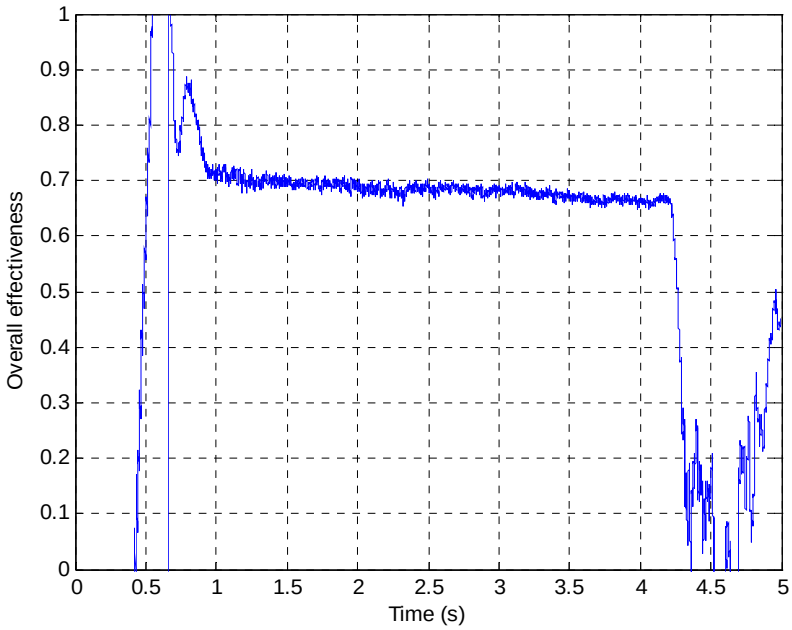


**Figure 18: Overall effectiveness with a decay of 3.5% between 1 to 4 seconds.**

**Table 1: Reynolds number, temperatures, overall effectiveness and heat flux at the beginning and end of run 10.**

| | 1450-3050ms | 3950-4050ms |
|---|---|---|
| **Re x10$^5$** | 1.66 | 1.44 |
| **Surface Temperature** | 320.5 K | 316.5 K |
| **Coolant Temperature** | 294.1 K | 289.4 K |
| **Freestream Temperature** | 378.7 K | 369.7 K |
| **Overall Effectiveness** | 0.6876 | 0.6626 |
| **Heat Flux** | 17230 W/m$^2$ | 9742.3 W/m$^2$ |

## *Overall Effectiveness*

**Table 2: Average characteristics for each run.**

| Run | Re x $10^5$ | Press Ratio | ID Coolant Temperature (K) | OD Coolant Temperature (K) | ID Massflow (kg/s) | OD Massflow (kg/s) | Freestream Temperature (K) |
|---|---|---|---|---|---|---|---|
| **2** | 1.59 | 1.499 | 226.1 | 220.6 | 1.2 | 0.801 | 337.5 |
| **10** | 1.44 | 1.522 | 226.6 | 223.3 | 1.107 | 0.7902 | 377.5 |
| **12** | 1.46 | 1.482 | 206.8 | 202.8 | 1.618 | 0.8836 | 373.9 |
| **21** | 1.71 | 1.5 | 1.59E+02 | 216.8 | 2.011 | 1.257 | 404.5 |

As stated previously in equation (4), the overall effectiveness is defined as

$$\phi = \frac{T_\infty - T_w}{T_\infty - T_c}$$

As is seen in Figure 18, the overall effectiveness was found to be relatively constant throughout the runs, decreasing just slightly as the Reynolds number decreased. A nearly constant overall effectiveness shows that the heat transfer mechanics were nearly steady in time. This result is important because it gives credibility to both engine designers in selecting a constant value for this parameter in their investigations and to the experimental facility for its ability to recreate accurate engine conditions. Figure 19 shows the same overall effectiveness trace as was shown in Figure 18 along with its accompanying surface, freestream and coolant temperature histories.

The overall effectiveness was found for all three cooling configurations for a variety of experiments. For each experiment the mass flow and temperature of the coolant varied, as well as the freestream Reynolds number. For this study runs 2, 10, 12, and 21 were analyzed. Table 2 displays the average characteristics which varied from run to run. The

inner and outer diameter coolant temperatures shown in the table are the average temperatures in the coolant tanks which fed the inner and outer diameter feed lines respectively. However, the coolant temperatures used in the calculation of the overall effectiveness were different for each airfoil used. Thermocouple readings at different sections of the coolant lines around the vane were used depending on their location relative to the airfoil being analyzed. The freestream temperature in the table is an average of the upstream temperatures measured by the rakes mentioned earlier. The freestream temperature used in the effectiveness calculation was a mean value of the measured upstream temperatures, which were found not to vary much between each other.

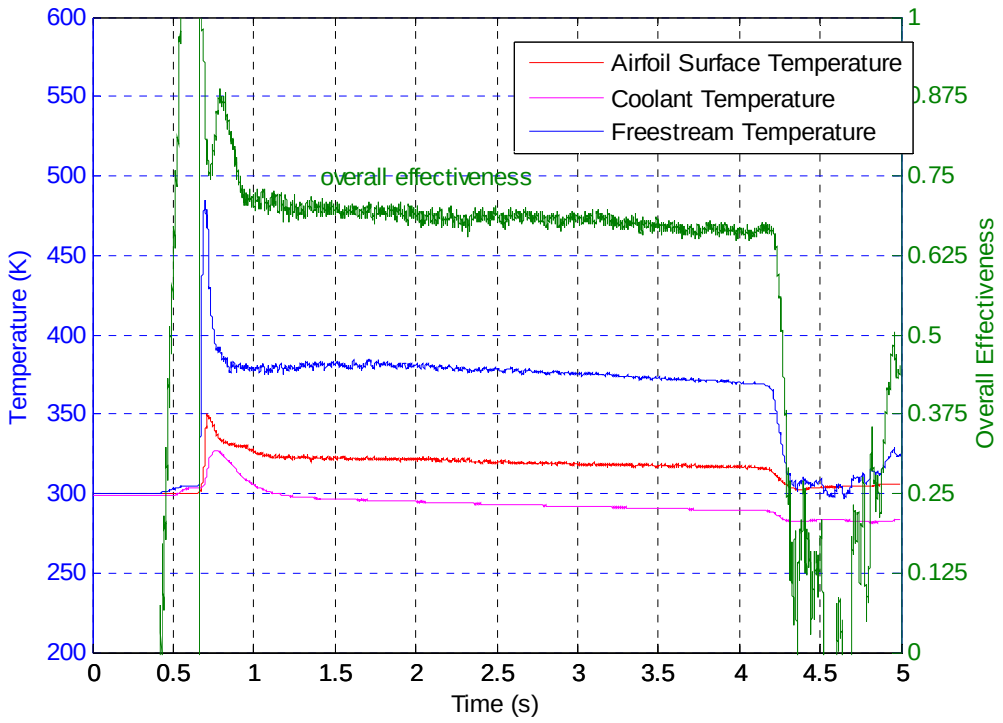


**Figure 19: Three temperature histories and their resultant overall effectiveness.**

The time varying overall effectiveness was found for gauges at 60% span and varying streamwise locations on both the suction and pressure surfaces. An average value of the overall effectiveness for each gauge was determined as the mean value for the time window when the heat transfer reached a steady value. For runs 2, and 10, this time window was between 1.5 to 4 seconds, and was between 2.5 to 4.5 seconds for run 21.

The relation of the streamwise average overall effectiveness to the mass flow for each airfoil type was investigated. Using the flow check information for each of the airfoils as shown in Figure 20 and Figure 21, an approximation of the coolant massflow to each airfoil could be determined. The pressure ratio shown in the figures was determined to be the ratio of the coolant pressure to an upstream static temperature. This static pressure was determined using the assumption of stagnation conditions in an isentropic flow and the relation:

$$\frac{P_o}{P} = (1 + \frac{\gamma - 1}{2} M^2)^{\gamma/(\gamma-1)} \tag{10}$$

Where $P_o$ is the measured upstream stagnation pressure, $\gamma$ is the specific heat ratio and M is the Mach number upstream. Solving this equation for P, the pressure ratio of the coolant to this static pressure could then be calculated. Using this ratio and interpolating the data in Figure 20 and Figure 21, the massflow to each particular airfoil could be estimated. Figure 22,Figure 23 andFigure 24 show how the averaged overall effectiveness and massflow vary at similar airfoil locations. From the figures, it is clear that the shaped hole airfoil has higher overall effectiveness values for lower massflows

than the multiple hole airfoil. The slot airfoil displayed similar massflow and effectiveness levels as the shaped airfoil.

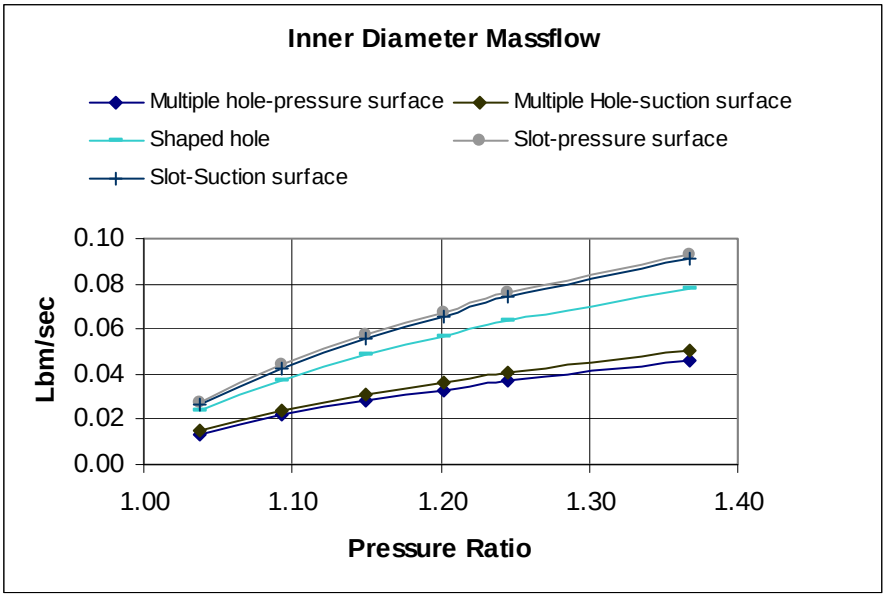


**Figure 20: Inner diameter massflow with respect to pressure ratio for each airfoil type.**

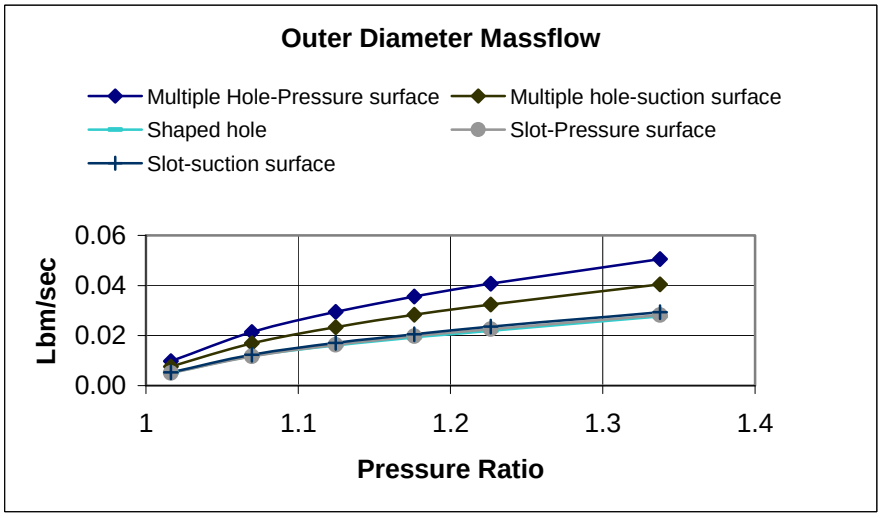


**Figure 21: Outer diameter massflow with respect to pressure ratio for each airfoil type**

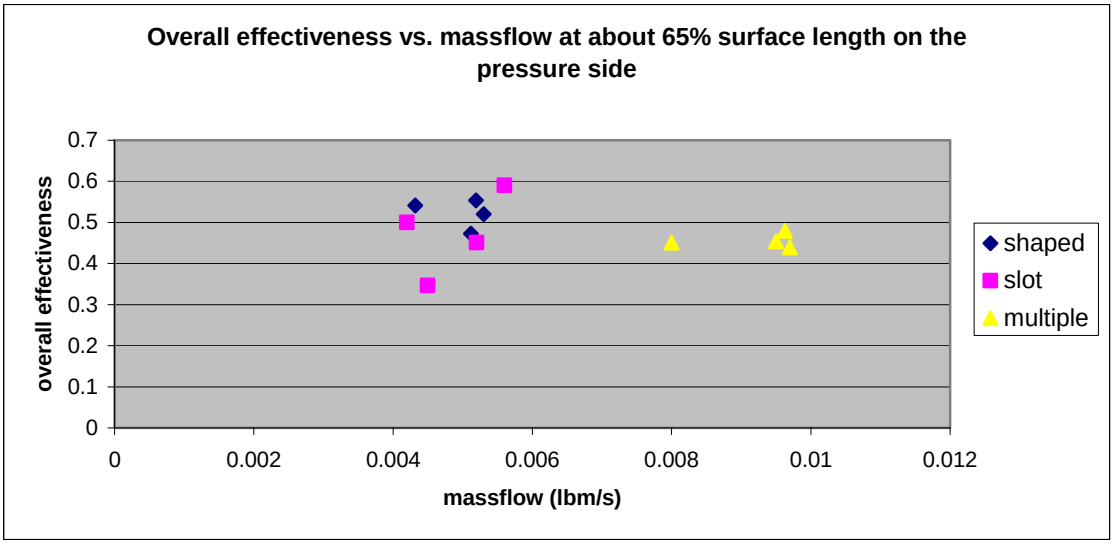


**Figure 22: Overall effectiveness variation with massflow at about 65% surface length on the pressure surface of the airfoils.**

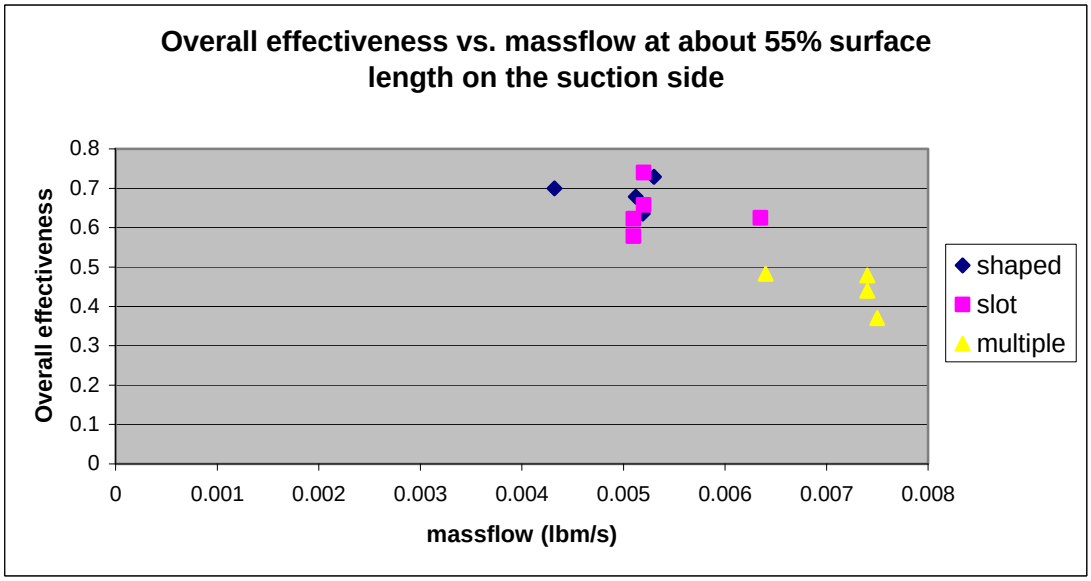


**Figure 23: Overall effectiveness variation with massflow at about 55% surface length on the suction surface of the airfoils.**

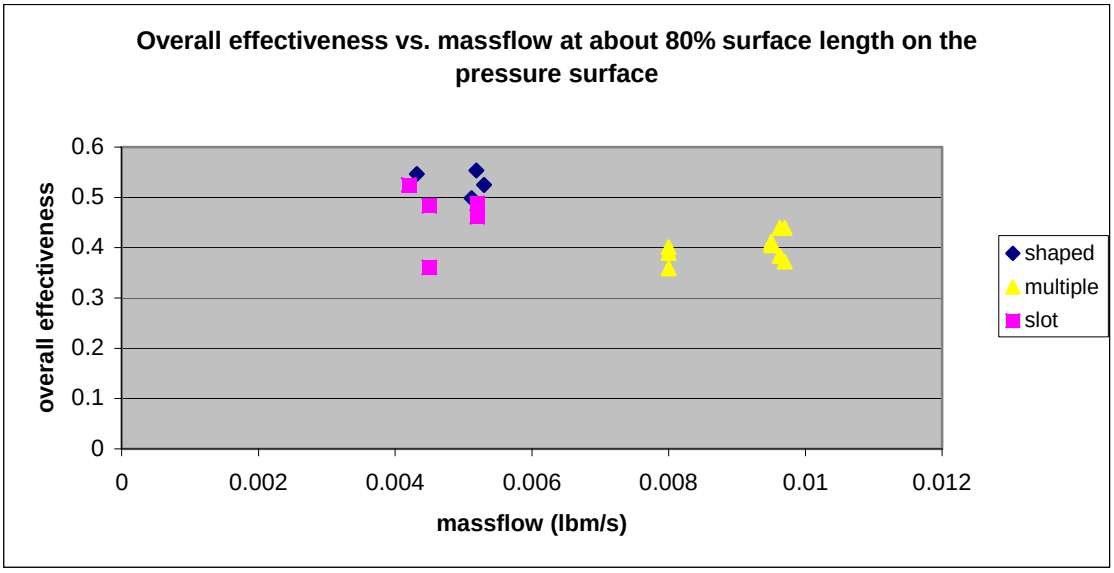


**Figure 24: Overall effectiveness variation with massflow at about 80% surface length on the pressure surface of the airfoils.**

The preceding figures show the shaped airfoil having a higher overall effectiveness for lower massflows at three similar airfoil locations than the multiple hole airfoil. Figure 25,Figure 26,Figure 27 andFigure 28 show the average overall effectiveness values at 60% span and varying streamwise locations. The figures show that the shaped hole airfoil has the consistently higher average overall effectiveness than the multiple hole airfoil across the streamwise locations for all four runs. There were too few working gauges on the slot for enough effectiveness calculations to be made in order to compare to the shaped and multiple hole airfoils at all streamwise locations. Appendix A shows the exact values for the effectiveness at their respective streamwise locations as well as the approximate massflow to each airfoil for each run.

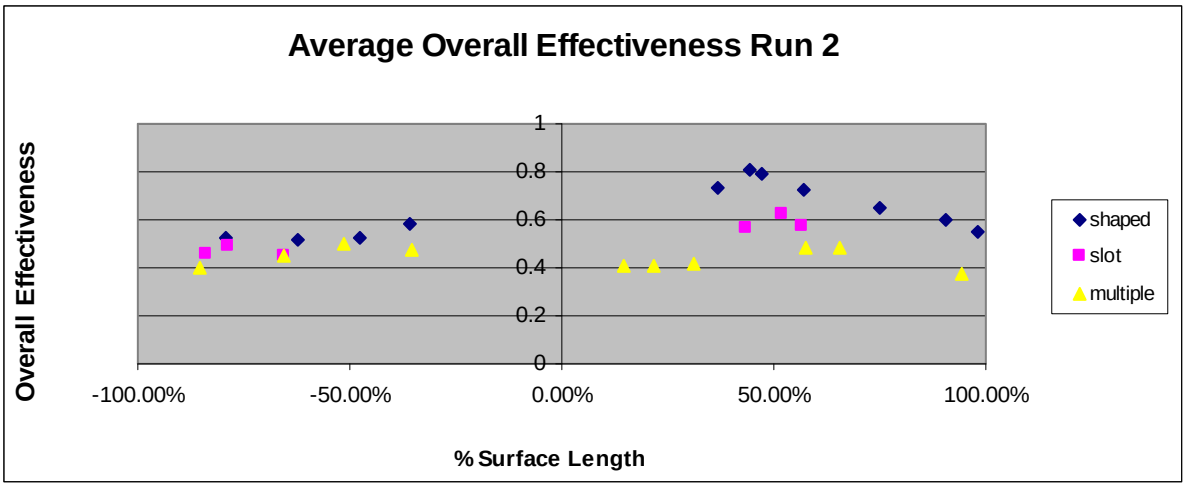


**Figure 25: Average overall effectiveness for run 2.**

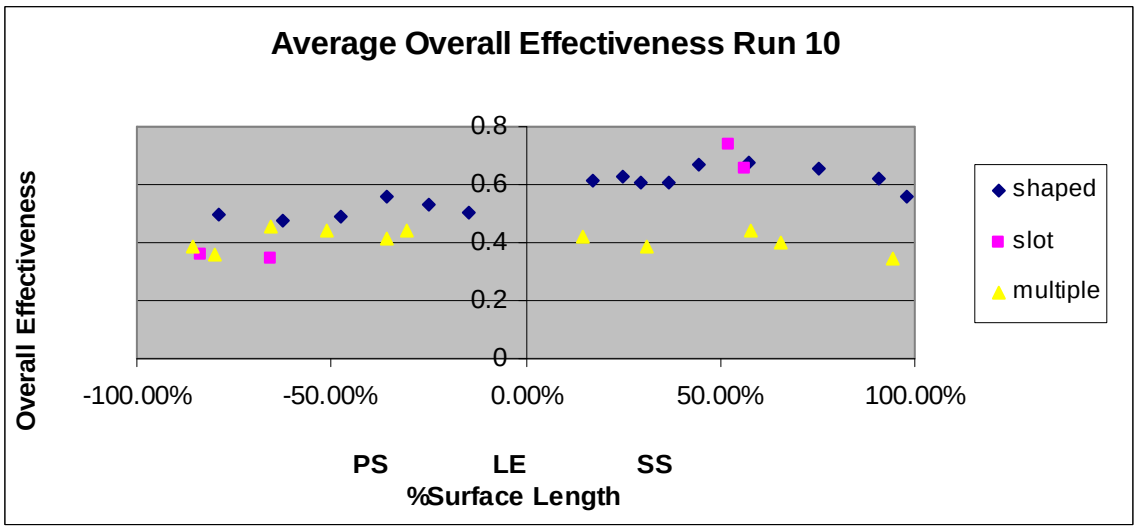


**Figure 26: Average overall effectiveness for run 10.**

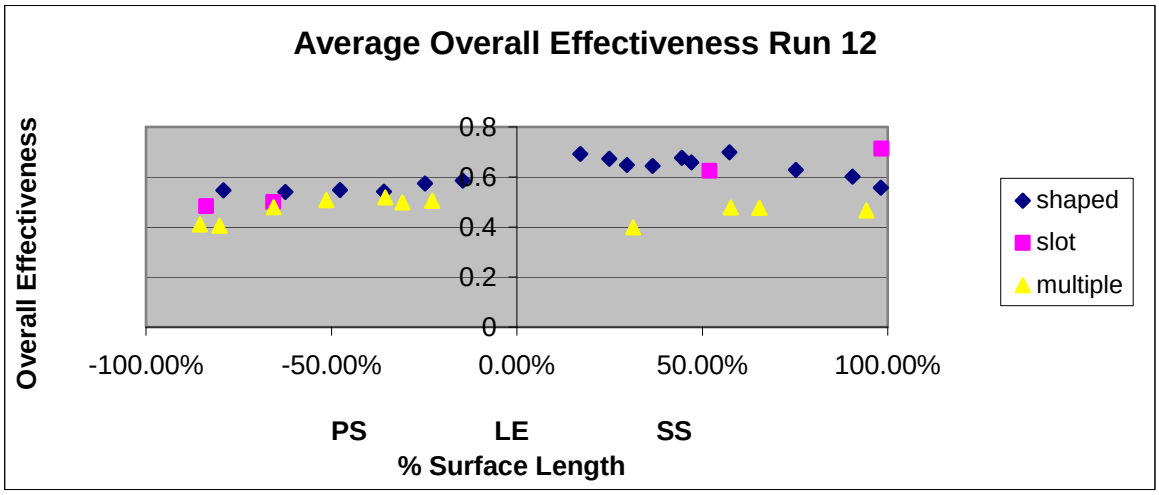


**Figure 27: Average overall effectiveness for run 12.**

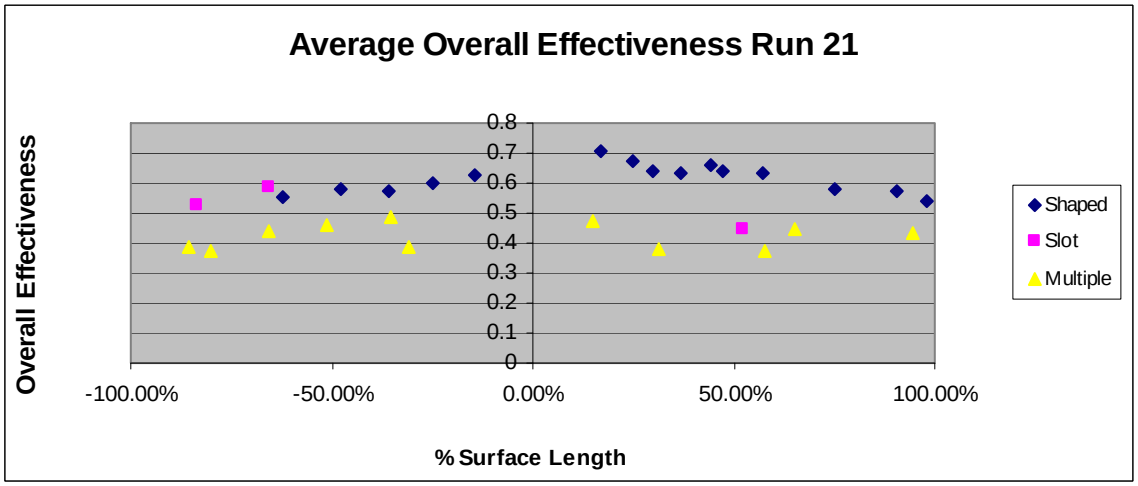


**Figure 28: Average overall effectiveness for run 21.**

# V: Conclusions and Recommendations

A study of the heat transfer in a true scale, fully cooled turbine vane ring under realistic engine conditions was conducted. Thin film heat transfer gauges at 60% span were used to measure surface temperatures at varying streamwise locations on three different film cooled turbine airfoils. Along with measurements of the freestream and coolant temperatures, the overall effectiveness could be calculated. The overall effectiveness was averaged for each gauge on each run, and plotted based on the particular airfoil the gauge was located on. An approximate massflow to each airfoil was determined using the flow check data shown in Figure 20 and Figure 21 and the flow characteristics for each run. It was shown in Figure 22,Figure 23 andFigure 24 that the shaped hole and slot airfoils had the highest overall effectiveness levels for lower mass flow rates than the multiple hole airfoil at 60% span and three different streamwise locations. As can be seen from the data in Appendix A, the shaped hole airfoil also had consistently higher values of effectiveness than the multiple hole airfoil over a range of streamwise locations. The streamwise effectiveness for the slot remains inconclusive due to the low number of working gauges on the airfoil on each run.

A comparison of the heat flux for each cooling configuration was made difficult due to the low number of thin film gauges that had an underlying thermocouple. It was shown in this study that the impulse response method requires a thermocouple within a close proximity a thin film gauge to minimize the error in measurement of the heat flux. Therefore a better analysis of how the heat flux varies over the surface of the airfoil as

well as between cooling techniques would require more thermocouples placed under thin film gauges at several airfoil locations. The disadvantages of such an analysis would be the difficulty of embedding such a large number of thermocouples into the airfoil surface at an exact location where the heat transfer gauge is located, and then having to measure both temperatures accurately. Another option could be to test the thermocouple superposition further by trying gauge and thermocouple pairs that are closer than what was tested in this study. With this, a more detailed knowledge of how the error in heat flux measurement varies with distance between the thin film gauge and thermocouple may be obtained.

# Appendix A: Average Overall Effectiveness

The following data shows the plots and exact values for the average overall effectiveness at varying streamwise locations. The tables also have the approximated coolant massflow to each airfoil.

## *Run 2*

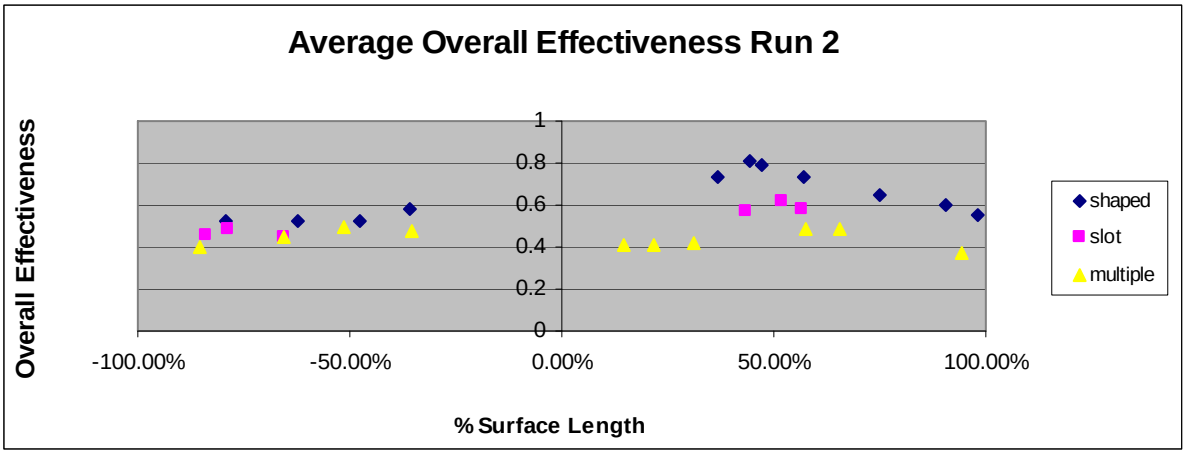


**Figure 29: Average overall effectiveness for run 2 at 60% span.**

**Table 3: Run 2 average effectiveness plotted on Figure 29.**

| Shaped-Holes | | |
|---|---|---|
| **% Surface Length** | **Avg. overall effectiveness** | **Massflow (lbm/s)** |
| **-79.10%** | 0.5245 | 0.0053 |
| **-62.40%** | 0.5201 | 0.0053 |
| **-47.70%** | 0.5223 | 0.0053 |
| **-35.80%** | 0.5848 | 0.0053 |
| **36.60%** | 0.7325 | 0.0053 |
| **44.50%** | 0.8048 | 0.0053 |
| **47.10%** | 0.7891 | 0.0053 |
| **57.30%** | 0.7288 | 0.0053 |
| **75.20%** | 0.65 | 0.0053 |
| **90.50%** | 0.604 | 0.0053 |
| **98.20%** | 0.5485 | 0.0053 |
| Slots | | |
| **% Surface Length** | **Avg. overall effectiveness** | **Massflow (lbm/s)** |
| **-83.80%** | 0.4614 | 0.0052 |
| **-78.60%** | 0.4878 | 0.0052 |
| **-65.70%** | 0.451 | 0.0052 |
| **43.40%** | 0.5706 | 0.0051 |
| **52.00%** | 0.622 | 0.0051 |
| **56.40%** | 0.578 | 0.0051 |
| Multiple holes | | |
| **% Surface Length** | **Avg. overall effectiveness** | **Massflow (lbm/s)** |
| **-85.40%** | 0.4006 | 0.008 |
| **-65.60%** | 0.4507 | 0.008 |
| **-51.40%** | 0.497 | 0.008 |
| **-35.50%** | 0.474 | 0.0154 |
| **14.70%** | 0.4097 | 0.017 |
| **21.90%** | 0.4088 | 0.017 |
| **31.30%** | 0.4173 | 0.017 |
| **57.70%** | 0.4826 | 0.0064 |
| **65.40%** | 0.4812 | 0.0064 |
| **94.30%** | 0.3732 | 0.0064 |

## *Run 10*

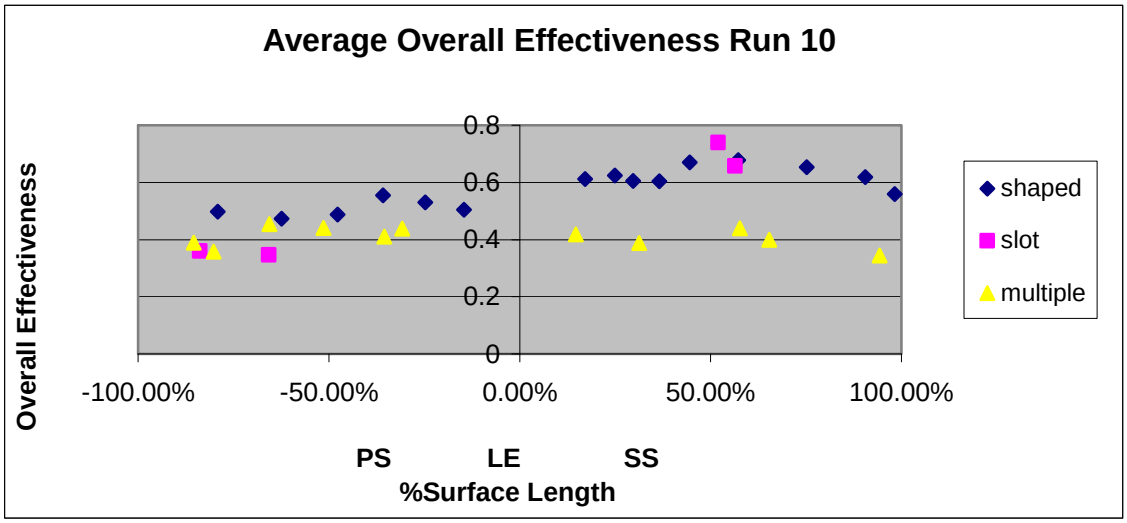


**Figure 30: Average overall effectiveness for run 10 at 60% span.**

**Table 4: Run 10 average overall effectiveness plotted on Figure 30.**

| Shaped-Holes | | |
|---|---|---|
| **% Surface Length** | **Avg. overall effectiveness** | **Massflow (lbm/s)** |
| **-79.10%** | 0.4984 | 0.00512 |
| **-62.40%** | 0.473 | 0.00512 |
| **-47.70%** | 0.4878 | 0.00512 |
| **-35.80%** | 0.5555 | 0.0229 |
| **-24.80%** | 0.5306 | 0.0229 |
| **-14.60%** | 0.5047 | 0.0229 |
| **17.10%** | 0.6115 | 0.0229 |
| **24.90%** | 0.6243 | 0.0229 |
| **29.70%** | 0.6049 | 0.0229 |
| **36.60%** | 0.6038 | 0.0229 |
| **44.50%** | 0.6698 | 0.00512 |
| **57.30%** | 0.6782 | 0.00512 |
| **75.20%** | 0.653 | 0.00512 |
| **90.50%** | 0.619 | 0.00512 |
| **98.20%** | 0.5596 | 0.00512 |
| Slots | | |
| **% Surface Length** | **Avg. overall effectiveness** | **Massflow (lbm/s)** |
| **-83.80%** | 0.3604 | 0.0045 |
| **-65.70%** | 0.3467 | 0.0045 |
| **52.00%** | 0.7394 | 0.0052 |
| **56.40%** | 0.6574 | 0.0052 |
| Multiple holes | | |
| **% Surface Length** | **Avg. overall effectiveness** | **Massflow (lbm/s)** |
| **-85.40%** | 0.3891 | 0.0095 |
| **-80.20%** | 0.3586 | 0.0095 |
| **-65.60%** | 0.454 | 0.0095 |
| **-51.40%** | 0.4404 | 0.0095 |
| **-35.50%** | 0.4104 | 0.01337 |
| **-30.80%** | 0.4384 | 0.01337 |
| **14.70%** | 0.4188 | 0.0147 |
| **31.30%** | 0.3882 | 0.0147 |
| **57.70%** | 0.4397 | 0.0074 |
| **65.40%** | 0.399 | 0.0074 |
| **94.30%** | 0.3448 | 0.0074 |

## *Run 12*

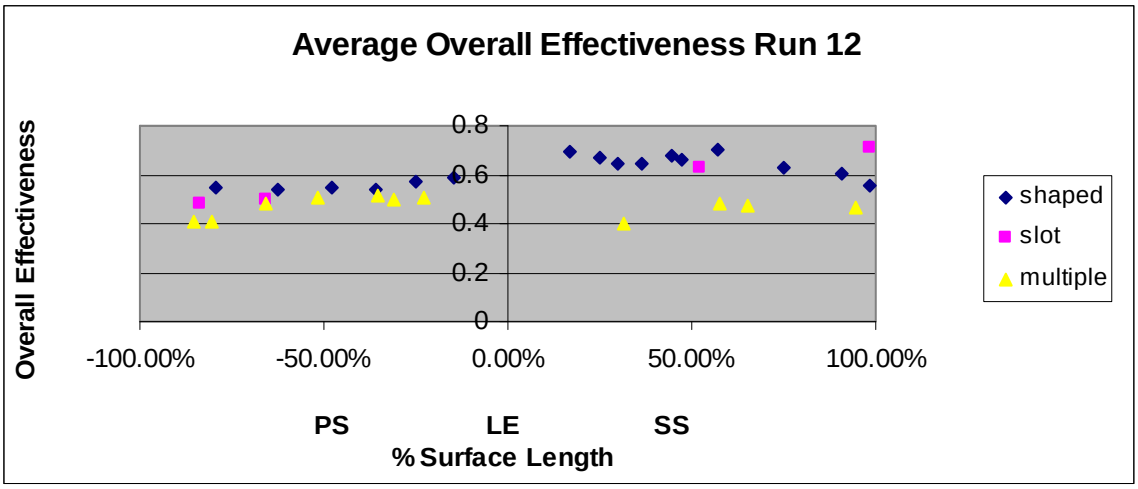


**Figure 31: Average overall effectiveness for run 12 at 60% span.**

**Table 5: Run 12 Average overall effectiveness plotted on Figure 31.**

| Shaped-Holes | | |
|---|---|---|
| **% Surface Length** | **Avg. overall effectiveness** | **Massflow (lbm/s)** |
| **-79.10%** | 0.5463 | 0.00432 |
| **-62.40%** | 0.5409 | 0.00432 |
| **-47.70%** | 0.5477 | 0.00432 |
| **-35.80%** | 0.5419 | 0.0233 |
| **-24.80%** | 0.5744 | 0.0233 |
| **-14.60%** | 0.5853 | 0.0233 |
| **17.10%** | 0.6928 | 0.0233 |
| **24.90%** | 0.6727 | 0.0233 |
| **29.70%** | 0.6477 | 0.0233 |
| **36.60%** | 0.6443 | 0.0233 |
| **44.50%** | 0.6771 | 0.00432 |
| **47.10%** | 0.6589 | 0.00432 |
| **57.30%** | 0.6993 | 0.00432 |
| **75.20%** | 0.6288 | 0.00432 |
| **90.50%** | 0.6018 | 0.00432 |
| **98.20%** | 0.5573 | 0.00432 |
| Slots | | |
| **% Surface Length** | **Avg. overall effectiveness** | **Massflow (lbm/s)** |
| **-83.80%** | 0.4829 | 0.0042 |
| **-65.70%** | 0.4995 | 0.0042 |
| **52.00%** | 0.6245 | 0.00635 |
| **98.30%** | 0.7125 | 0.00635 |
| Multiple holes | | |
| **% Surface Length** | **Avg. overall effectiveness** | **Massflow (lbm/s)** |
| **-85.40%** | 0.411 | 0.00963 |
| **-80.20%** | 0.405 | 0.00963 |
| **-65.60%** | 0.4797 | 0.00963 |
| **-51.40%** | 0.5078 | 0.00963 |
| **-35.50%** | 0.5181 | 0.0115 |
| **-30.80%** | 0.4993 | 0.0115 |
| **-22.80%** | 0.5049 | 0.0115 |
| **31.30%** | 0.399 | 0.0127 |
| **57.70%** | 0.4784 | 0.0074 |
| **65.40%** | 0.4769 | 0.0074 |
| **94.30%** | 0.466 | 0.0074 |

## *Run 21*

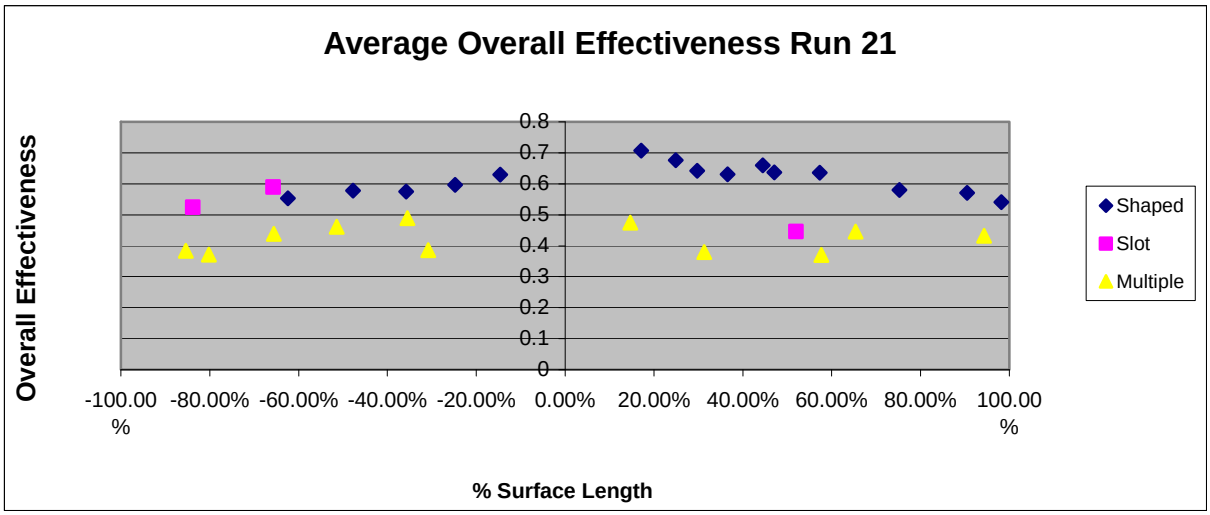


**Figure 32: Average overall effectiveness for run 21 at 60% span.**

**Table 6: Run 21 average overall effectiveness plotted on Figure 32.**

| Shaped-Holes | | |
|---|---|---|
| **% Surface Length** | **Avg. overall effectiveness** | **Massflow (lbm/s)** |
| **-79.10%** | | 0.00519 |
| **-62.40%** | 0.5534 | 0.00519 |
| **-47.70%** | 0.5785 | 0.00519 |
| **-35.80%** | 0.5748 | 0.023 |
| **-24.80%** | 0.597 | 0.023 |
| **-14.60%** | 0.6294 | 0.023 |
| **17.10%** | 0.7067 | 0.023 |
| **24.90%** | 0.6765 | 0.023 |
| **29.70%** | 0.6423 | 0.023 |
| **36.60%** | 0.6311 | 0.023 |
| **44.50%** | 0.6592 | 0.00519 |
| **47.10%** | 0.6369 | 0.00519 |
| **57.30%** | 0.6355 | 0.00519 |
| **75.20%** | 0.5802 | 0.00519 |
| **90.50%** | 0.5713 | 0.00519 |
| **98.20%** | 0.5407 | 0.00519 |
| Slots | | |
| **% Surface Length** | **Avg. overall effectiveness** | **Massflow (lbm/s)** |
| **-83.80%** | 0.5244 | 0.0056 |
| **-65.70%** | 0.5899 | 0.0056 |
| **52.00%** | 0.4459 | 0.0059 |
| **56.40%** | | 0.0059 |
| Multiple holes | | |
| **% Surface Length** | **Avg. overall effectiveness** | **Massflow (lbm/s)** |
| **-85.40%** | 0.3838 | 0.0097 |
| **-80.20%** | 0.372 | 0.0097 |
| **-65.60%** | 0.439 | 0.0097 |
| **-51.40%** | 0.461 | 0.0097 |
| **-35.50%** | 0.4889 | 0.0179 |
| **-30.80%** | 0.3864 | 0.0179 |
| **14.70%** | 0.475 | 0.0196 |
| **21.90%** | | 0.0196 |
| **31.30%** | 0.3795 | 0.0196 |
| **57.70%** | 0.3702 | 0.0075 |
| **65.40%** | 0.4456 | 0.0075 |
| **94.30%** | 0.4327 | 0.0075 |

# Appendix B: Derivation of the Impulse Response Method

The following derivation of the impulse response method was performed by Doorly and Oldfield in the paper entitled *The Theory of Advanced Multi-Layered Thin Film Heat Transfer Gauges*, located in the International Journal of Heat and Mass Transfer, volume 30, number 6, pages 1159 to 1168.

The relationship between the heat transfer rate $q$ and the surface temperature $T_s$ for any system is defined as:

$$q = F(s)T_s \tag{11}$$

For the double-sided model used in this study:

$$F(s) = (\rho_1 c_1 k_1 s)^{1/2} \frac{(1 - A\exp\{-2a(s/\alpha_1)^{1/2}\})}{(1 + A\exp\{-2a(s/\alpha_1)^{1/2}\})} \tag{12}$$

Where $c$ is the specific heat capacity of the gauge, $a$ is the gauge thickness, $\alpha$ is diffusivity of the gauge, $k$ is the thermal conductivity of the gauge, and $s$ the Laplace transform variable. To measure surface heat transfer rates, a constant current is passed through the thin film gauge, and the change in voltage v caused by a change in surface temperature is given by

$$v = v_0 \beta T \tag{13}$$

Where $\beta$ is the temperature coefficient of resistance of the film. The voltage output from the analog is given by

$$v_a = \frac{v_0}{k_a} s^{1/2} \beta T_s \tag{14}$$

Where $v_0$ is the initial film voltage and $k_a$ is the analog calibration constant. Combining equations ((11) to ((14) yields

$$q = \frac{k_a}{v_0} \frac{F(s)}{\beta s^{1/2}} v_a \tag{15}$$

If the analog output is a unit step of $v_a$, and for short times, the heat transfer rate can be written as

$$q = \frac{1}{\beta} \frac{k_a}{v_0} h(t) (\rho_1 c_1 k_1)^{1/2} \tag{16}$$

Where $h(t)$ is the gauge step calibration function, or impulse response function with a Laplace transform

$$H(s) = \frac{F(s)}{(\rho_1 c_1 k_1)^{1/2} s^{3/2}} \tag{17}$$

The sampled analog output signal, with Laplace transform is

$$v_a = \frac{v_0}{k_a} s^{1/2} T_s \alpha$$

Can be considered to be a series of step functions such that

$$v_a(N\tau) = \sum_{n=1}^{N} a_n u(N\tau - n\tau) \tag{18}$$

Where $u(t-\tau)$ is the delayed unit step function. Since $e^{-\tau s}F(s)$ is the Laplace transform of $f(t-\tau)$, where $F(s)$ is the Laplace transform of $f(t)$, the transform of equation (18) is

$$v_a = \sum_{n=1}^{N} a_n \frac{e^{-st_n}}{s}$$

Where

$$t_n = n\tau$$

and

$$a_n = v_a(n\tau) - v_a(n-1)\tau \tag{19}$$

Then

$$\dot{q} = \frac{1}{\alpha}\frac{k_a}{v_0} H(s)(\rho_1 c_1 k_1)^{1/2} v_a(s) \tag{20}$$

So for $v_a$ a sum of the series of step functions

$$\dot{q}_s(s) = \frac{1}{\alpha}\frac{k_a}{v_0} H(s)(\rho_1 c_1 k_1)^{1/2} \sum_{n=1}^{N} a_n e^{-st_n} \tag{21}$$

And inverting equation (21) yields

$$\dot{q}(N\tau) = \frac{1}{\alpha}\frac{k_a}{v_0}(\rho_1 c_1 k_1)^{1/2} \times \sum_{n=1}^{N} h(N-n)\tau(v_a(n\tau) - v_a(n-1)\tau) \tag{22}$$

So if $h(n\tau)$ is known at $N$ discrete points, then $q_s(N\tau)$, the sampled heat transfer signal can be computed. For two-layered gauges used in this study, from equation (12),

$$F(s) = (\rho_1 c_1 k_1 s)^{1/2} \frac{(1 - A\exp\{-2a(s/\alpha_1)^{1/2}\})}{(1 + A\exp\{-2a(s/\alpha_1)^{1/2}\})}$$

Therefore

$$H(s) = \frac{1}{s}\frac{(1 - A\exp\{-2a(s/\alpha_1)^{1/2}\})}{(1 + A\exp\{-2a(s/\alpha_1)^{1/2}\})} \tag{23}$$

Expanding the denominator yields

$$H(s) = \frac{1}{s}(1 + 2\sum_{m=1}^{\infty}(-1)^m A^m \times \exp(-2ma(s/\alpha_1)^{1/2})) \tag{24}$$

And inverting this results in the impulse response function

$$h(t) = 1 + 2\sum_{m=1}^{\infty}(-1)^m A^m erfc(ma/(\alpha_1 t)^{1/2}) \tag{25}$$

For this study, the impulse response function was found for 100,000 points. It need only be solved for once because the same gauges were used on all airfoils and on every run.

Bibliography

Anthony, R.J., Jones, T.V., Oldfield, M.L.G., LaGraff, J.E., "Development of High Density Arrays of Thin Film Heat Transfer Gauges," *Proceedings of the 5th ASME/JSME Thermal Engineering Joint Conference*, ASME, 1999.

Barringer, M.D., Thole, K.A., Polanka, M.D., "Effects of Combustor Exit Profiles on High Pressure Turbine Vane Aerodynamics and Heat Transfer," *Proceedings of the ASME Turbo Expo 2006: Power for Land, Sea and Air*, ASME, 2006.

Barthet, S., Kulisa, P., "Numerical Investigation of Film Cooling Flow Induced by Cylindrical and Shaped Holes," *Annals of the New York Academy of Sciences*, Volume 934, 2001.

Bogard, D.G., Thole, K.A., "Gas Turbine Film Cooling," *Journal of Propulsion and Power*, December 2005.

Bunker, R.S., "Effectiveness Due to Discrete Holes in a Transverse Surface Slot," *Proceedings of the 2002 IGTI Turbo Expo: International Gas Turbine Conference and Exposition*, Amsterdam, June, 2002.

Bunker, R.S., "A Review of Shaped Hole Turbine Film Cooling Technology," *Journal of Heat Transfer*, ASME, 2005.

Kays, W.M., Crawford, M.E., *Convective Heat and Mass Transfer*, McGraw-Hill, New York, 1987.

Dally, J.M., Riley, W.F., McConnell, K.G., *Instrumentation for Engineering Measurements*, New Jersey, John Wiley and Sons, 1993.

Dittmar, J., Jung, I.S., Schulz, A., Wittig, S., Lee, J.S., "Film Cooling from Rows of Holes- Effect of Cooling Hole Shape and Row Arrangement on Adiabatic Effectiveness," *Annals of the New York Academy of Sciences*, Volume 934, 2001.

Doorly, J.E., Oldfield, M.L.G., "The Theory of Advanced Multi-Layer Thin Film Heat Transfer Gauges," *International Journal of Heat and Mass Transfer*, Volume 30, Number 6, 1986.

Gritsch, M., Schulz, A., Wittig, S., "Adiabatic Wall Effectiveness Measurements of Film-Cooling Holes With Expanded Exits," *International Gas Turbine & Aeroengine Congress and Exhibition*, ASME, June 1997.

Mouzon, B.D., Albert, J.E., Terrell, E.J., Bogard, D.G., "Net Heat Flux Reduction and Overall Effectiveness for a Turbine Blade Leading Edge," *ASME Turbo Expo 2005: Power for Land, Sea, and Air*, Reno, Nevada, June 2005.

Oldfield, M.L.G., "Impulse Response Processing of Transient Heat Transfer Gauge Signals," *ASME Turbo Expo 2006: Power for Land, Sea, and Air*, Barcelona, Spain, May 2006.

Rutledge, J.L., Robertson, D., Bogard, D.G., *Degradation of Film Cooling Performance on a Turbine Vane Suction Surface due to Surface Roughness*, Journal of Turbomachinery, Volume 128, pp. 547-554, July 2006.

Saravanamuttoo, H.I.H., Rogersl, G.F.C., Cohen, H., *Gas Turbine Theory*, Pearson Education Limited, Essex, England, 2001.

Sargison, J.E., Guo, S.M., Oldfield, M.L.G., Rawlinson, A.J., "The Variation of Heat Transfer Coefficient, Adiabatic Effectiveness and Aerodynamic Loss with Film Cooling Hole Shape," *Annals of the New York Academy of Sciences*, Volume 934, 2001.

Schmidt, D.L., Sen, B., Bogard, D.G., "Film Cooling with Compound Angle Holes: Adiabatic Effectiveness," *Journal of Turbomachinery*, Volume 118, pp. 807-813, October 1996.

Schulz, A., "Combustor Lining Cooling Technology in Scope of Reduced Pollutant Formation and Rising Thermal Efficiencies," *Annals of the New York Academy of Sciences*, Volume 934, 2001.

Sen, B., Schmidt, D.L., Bogard, D.G., "Film Cooling with Compound Angle Holes: Heat Transfer," *Journal of Turbomachinery*, Volume 118, pp. 800-805, October 1996.

Suslov, D., Schulz, A., Wittig, S., "Effect of Reynolds Number, Turbulence Level and Periodic Wake Flow on Heat Transfer on Low Pressure Turbine Blades," *Annals of the New York Academy of Sciences*, Volume 934, 2001.

Sweeney, P.C., Rhodes, J.F., "An Infrared Technique of Evaluating Turbine Airfoil Cooling Designs," *Journal of Turbomachinery*, Volume 122, pp. 170-177, January 2000.

# REPORT DOCUMENTATION PAGE

*Form Approved*
*OMB No. 074-0188*

The public reporting burden for this collection of information is estimated to average 1 hour per response, including the time for reviewing instructions, searching existing data sources, gathering and maintaining the data needed, and completing and reviewing the collection of information. Send comments regarding this burden estimate or any other aspect of the collection of information, including suggestions for reducing this burden to Department of Defense, Washington Headquarters Services, Directorate for Information Operations and Reports (0704-0188), 1215 Jefferson Davis Highway, Suite 1204, Arlington, VA 22202-4302. Respondents should be aware that notwithstanding any other provision of law, no person shall be subject to an penalty for failing to comply with a collection of information if it does not display a currently valid OMB control number.
**PLEASE DO NOT RETURN YOUR FORM TO THE ABOVE ADDRESS.**

| 1. REPORT DATE *(DD-MM-YYYY)* | 2. REPORT TYPE | 3. DATES COVERED *(From – To)* |
|---|---|---|
| 14 Jun 07 | **Master's Thesis** | **June 2006– Jun 2007** |

**4. TITLE AND SUBTITLE**

A Comparison of Film Cooling Techniques in a High Speed, True Scale, Fully Cooled Turbine Vane Ring.

**5a. CONTRACT NUMBER**

**5b. GRANT NUMBER**

**5c. PROGRAM ELEMENT NUMBER**

**6. AUTHOR(S)**

Umholtz, Michael, J., Ensign, USN

**5d. PROJECT NUMBER**

**5e. TASK NUMBER**

**5f. WORK UNIT NUMBER**

**7. PERFORMING ORGANIZATION NAMES(S) AND ADDRESS(S)**

Air Force Institute of Technology
Graduate School of Engineering and Management (AFIT/EN)
2950 Hobson Way
WPAFB OH 45433-7765

**8. PERFORMING ORGANIZATION REPORT NUMBER**

**AFIT/GAE/ENY/07-J21**

**9. SPONSORING/MONITORING AGENCY NAME(S) AND ADDRESS(ES)**

AFRL/TRF
Attn: Dr. Marcus Polanka
2950 Hobson Way
Wright Patterson, OH 45433-7765 DSN: (937) 785-3636

**10. SPONSOR/MONITOR'S ACRONYM(S)**

**11. SPONSOR/MONITOR'S REPORT NUMBER(S)**

**12. DISTRIBUTION/AVAILABILITY STATEMENT**

APPROVED FOR PUBLIC RELEASE; DISTRIBUTION UNLIMITED.

**13. SUPPLEMENTARY NOTES**

**14. ABSTRACT**

An effort was undertaken to understand the impact of different film cooling configurations in a true scale turbine vane for three proprietary airfoil designs. The measurements for this study were taken at the United States Air Force Turbine Research Facility (TRF). The TRF enabled heat transfer data to be obtained on full scale turbine hardware under realistic engine conditions. The surface heat flux of the turbine blades was analyzed using the impulse response method. The overall effectiveness was compared between airfoil types at 60% span over varying streamwise locations on both suction and pressure surfaces. Using an approximated massflow, a comparison of the overall effectiveness with respect to massflow rate could be made between airfoils at three different airfoil locations. The shaped hole and slot cooling configurations were found to have higher average overall effectiveness for lower massflow rates than the multiple hole configuration based on the conditions tested.

**15. SUBJECT TERMS**

Turbine research facility, film cooling, impulse response method, overall effectivness

| 16. SECURITY CLASSIFICATION OF: | | | 17. LIMITATION OF ABSTRACT | 18. NUMBER OF PAGES | 19a. NAME OF RESPONSIBLE PERSON |
|---|---|---|---|---|---|
| REPORT | ABSTRACT | c. THIS PAGE | | | Dr. Mark Reeder (AFIT/ENY) |
| **U** | **U** | **U** | **UU** | 63 | **19b. TELEPHONE NUMBER** *(Include area code)* (937) 785-3636, ext 4530; e-mail: Mark.Reeder@afit.edu |

**Standard Form 298 (Rev: 8-98)** Prescribed by ANSI Std. Z39-18